On the kinetic energy spectrum of atmospheric motions in the planetary boundary layer

Lundtang Petersen, Erik

Publication date:
1975

Document Version
Publisher's PDF, also known as Version of record

Risø Report No. 285

Risø Report No. 285

Danish Atomic Energy Commission

Research Establishment Risø

On the Kinetic Energy Spectrum of Atmospheric Motions in the Planetary Boundary Layer

by Erik Lundtarg Petersen

January 1975

Sales distributors: Jul. Gjellerup, 17, Sølvgade, DK-1307 Copenhagen K, Denmark

Available on exchange from: Library, Danish Atomic Energy Commission, Risø, DK-4000 Roskilde, Denmark

January 1975 Risø Report No. 285

On the Kinetic Energy Spectrum of Atmospheric Motions in the Planetary Boundary Layer

by

Erik Lundtang Petersen

The Danish Atomic Energy Commission
Research Establishment Risø
Physics Department

UDC 551.55

Abstract

Kinetic energy spectra of the horizontal wind vector were estimated from time series measured along the Risø 123 m meteorological tower throughout ten years. Also measurements from other localities (Station Nord, Greenland, and Karlstrup, Zealand) were used. Spectra and methods are presented and discussed. Emphasis is laid on the gain in information which is achieved when the components of the wind vector are considered rather than just the wind speed.

Spectral equations in the frequency domain are derived from the equations of motion. It is shown how a ratio including the Coriolis parameter, the quadrature spectrum of the components, the energy spectrum, and the frequency can be used to determine the explicit effect of the rotating of the earth on the kinetic energy spectrum.

The wind structure in the boundary layer, as measured at the Risø site, and its relation to the diurnal cycle and horizontal inhomogeneities of surface temperature are investigated. The data reveal an exceptionally large turning of the wind with the height above the ground. It is shown that this feature can be given a phenomenological description by making an analogy to the thermal-wind effect.

ISBN 87 550 0318 4

CONTENTS

		Page
Preface		5
List of Symbols		6
1.	Introduction	7
2.	Analysis of Atmospheric Variables, Theory	8
	2.1. Random Functions	8
	2.1.1. Second Order Moments	9
	2.1.2. Spectral Representation in Wave Number Space	10
	2.1.3. Spectral Representation in Frequency Space	12
	2.1.4. The One-Dimensional Wave Number Spectrum -Tensor	13
	2.2. The Eddy Concept	14
	2.3. Taylor's Hypothesis	15
	2.4. The Limits of Atmospheric Spectra	16
	2.5. The Graphical Representation of Spectra	17
	2.6. Reynolds Convention	19
3.	The Data Records	20
	3.1. Introduction	20
	3.2. The Rise Records	20
	3.3. The Karlstrup Record	22
	3.4. The Station Nord Record	23
4.	Practical Spectral Analysis	26
	4.1. The FFT	28
	4.2. The Discrete Fourier Transform	28
	4.3. Problems in Digital Spectral Analyses	29
	4.4. Smoothing	30
	4.5. Missing Observations	31
5.	Spectra of the Horizontal Wind Vector	32
	5.1. Introduction	32
	5.2. Composite Spectra	32
	5.2.1. The Spectral Gap	35
	5.2.2. An Explanation of the Spectral Gap	43
	5.3. The True Periodicities in the Spectrum	44
	5.4. Speed Spectra versus Component Spectra	49
	5.5. The Effects on the Component Spectra caused by a Rotation of the Coordinate System	57

Page

6. Spectral Equations in the Frequency Domain 61
6.1. The Governing Equations 61
6.2. The Spectral Equations 62
6.3. Discussion of the Spectral Equations 66
6.3.1. The Influence of the Rotating of the Earth 67
7. Daily Variation of Meteorological Elements 73
7.1. The Planetary Boundary Layer 73
7.2. The Boundary Layer Equations 74
7.3. Analytical Solutions to the Equations 77
7.4. Numerical Modelling of the Planetary Boundary Layer .. 77
7.5. Deductions from Measured Mean Profiles Using the Principle of Equilibrium Motion 79
Summary and Conclusions 98
Acknowledgements 99
References 100

PREFACE

The source of virtually all the energy of the atmosphere is solar energy. When radiation is absorbed at the surface of the earth and in the atmosphere, it appears as internal energy which is converted into other atmospheric forms such as potential, kinetic, and latent energy.

One of the major tasks in the atmospheric sciences is to determine how transformation, exchange and transportation of different forms of energy are carried out in the atmosphere. The ultimate goal is the complete understanding of the mechanisms responsible for the way in which the atmosphere organizes itself. This understanding is essential for successful weather forecasting and modelling of our atmospheric environment.

It is the purpose of this report to provide information on the structure of the atmospheric kinetic energy through analysis of measured time series of atmospheric parameters.

LIST OF SYMBOLS

Brackets denote ensemble averaging, e.g. $\langle u \rangle$
An overbar denotes time averaging, e.g. $\overline{u}$
An underbar denotes a vector, e.g. $\underline{u}$
The Fourier transform of u can be denoted by $\hat{u}$

If not otherwise indicated, the coordinate system is a right-handed Cartesian coordinate system rotating with the earth, and arranged so that the x_3-axis is antiparallel to the acceleration due to gravity.

The notations x_1, x_2, and x_3 are used alternatively with x, y, and z in order to obtain the convenience which Einstein's summation convention affords, but still to retain the possibility of being in accordance with ordinary micrometeorological usage where convenient.

Einstein's summation convention implies summation over repeated indices, e.g., $u_i u_i = u_1 u_1 + u_2 u_2 + u_3 u_3$.

$\underline{i}_i$	unit vector in the i^{th} direction
$\underline{u}$	velocity vector, $\underline{u} = \underline{i}_1 u_1 + \underline{i}_2 u_2 + \underline{i}_3 u_3$
u_i	i^{th} component of velocity
u, v, w	(x_1, x_2, x_3) and (x, y, z) components of velocity
V, v	magnitude of the horizontal wind vector
p	pressure
ρ	density
T	temperature; absolute when indicated
ν	kinematic viscosity
g	acceleration due to gravity
f	the Coriolis parameter = $2\Omega\sin\varphi$, where Ω is the angular frequency of the earth's rotation and φ is the latitude
ε	average dissipation rate of turbulent kinetic energy per unit mass
ε_{ijk}	alternating tensor: $\varepsilon_{ijk} = 1$, if (i, j, k) = (1, 2, 3), (2, 3, 1), or (3, 1, 2) $\varepsilon_{ijk} = 0$, if i, j, and k are not all different $\varepsilon_{ijk} = -1$, if (i, j, k) = (3, 2, 1), (2, 1, 3), or (1, 3, 2)

Other symbols are used in this report; their meaning is given in the text where they occur.

1. INTRODUCTION

Many of the parameters describing the state of the atmosphere such as wind speed, pressure, and temperature are functions of positions in space and of time. At a given time their values vary from point to point, and, at a given point in space, their values vary in time.

To undertake our task ideally, observations of all relevant parameters should be available every millimeter all around the globe at all times. Such observations are not available. For the first, we cannot measure all the relevant parameters known to us, and those we can measure, we cannot measure with such a density; secondly, we are not sure that we know all the relevant parameters to measure; and thirdly, all measurements are bound to be within certain time and space limits.

The observations of meteorological elements often prove to be so irregular that any attempt to give them a precise analytical description is quite hopeless; therefore it is expedient to use a statistical description, considering the physical processes as random (stochastic) processes and the observations as random (stochastic) functions.

In the analysis of random functions some of the most useful tools are orthogonal decompositions, the reason being that orthogonal decomposition corresponds to the introduction of a general form of cartesian frames of reference which allow the use of a general form of Pythagorean relation. In physics, the most important orthogonal decomposition is the harmonic one because the amount of explained variance is plotted versus frequency or wavenumber, and hence makes direct reference to time or length scales in the process being studied. Another important aspect of the harmonic (Fourier) decomposition is that it is the only decomposition that does not tie the process under consideration to any origin or epoch, but is invariant under a displacement of time in the limit where the memory of the process becomes small compared to the time over which the process is considered.

As said by Wiener in 1949, "This mode of invariance under a translation of the origin of time simply asserts the repeatability of the method and is indeed a necessary condition for the existence of any scientific theory whatever. A scientific theory bound to an origin in time, and not freed from it by some mathematical technique, is a theory in which there is no legitimate inference from the past to the future".

Thus, we are inevitably led to the theory of stationary random processes and their spectral decomposition. This theory requires a fairly elaborate mathematical technique, which is now amply described in the literature

(N. Wiener, 1949, M. Loeve, 1955, A.M. Yaglom, 1962, I.S. Bendat and A.G. Piersol, 1966, E.I. Hannan, 1970, H. Cramer and M.R. Leadbetter, 1960, J.L. Lumley and H.A. Panofsky, 1964, J.L. Lumley, 1970). In the next chapter (2) we establish a frame of references but emphasize that even an explanation of the fundamentals of the theory is beyond the scope of this report. Further, chapter 2 contains discussions of the relations between time spectra, space spectra, and eddy sizes of turbulent motions.

In chapter 3 information is given concerning how, when, and where the analysed time series were obtained. Chapter 4 describes the practical implications of digital spectral analysis, and in chapter 5 the measured energy spectra of the horizontal wind vector are presented and discussed. The equations governing atmospheric motions are used in chapter 6 to derive a spectral equation in the frequency domain in the hope of unfolding more of the information contained in the shapes of measured time spectra of kinetic energy.

Finally, chapter 7 is devoted to the thermally introduced periodicities found in time series of the horizontal wind vector in the planetary boundary layer.

2. ANALYSIS OF ATMOSPHERIC VARIABLES, THEORY

2.1. Random Functions

Defining a random function, we can think of a series of measurements of a given random process

$$\underline{i}_1 \xi_1 \ (\underline{x}, t) = \underline{i}_1 \xi_1 \ (\underline{x}, t) + \underline{i}_2 \xi_2 \ (\underline{x}, t) + \ldots . + \underline{i}_n \xi_n \ (\underline{x}, t) + \ldots$$

under identical curcumstances. In this report we shall always think of $\underline{i}_i \xi_i (\underline{x}, t)$ as a wind vector if not otherwise indicated ($i = 1, 2, 3$). If $\underline{i}_i$ and the index i are removed, we speak of scalars such as temperature and wind speed; t is time ($-\infty < t < \infty$) and $\underline{x} = (x_1, x_2, x_3)$ is a point in the three-dimensional Euclidean space. Each measurement correspondt to a different function

$$\underline{i}_i \xi_i^{(1)} \ (\underline{x}, t), \ \underline{i}_i \xi_i^{(2)} \ (\underline{x}, t), \ \ldots . , \ \underline{i}_i \xi_i^{(n)} \ (\underline{x}, t), \ldots$$

and we say that the measurements are realizations of the random process $\underline{i}_i \xi_i (\underline{x}, t)$. The collection of functions $\underline{i}_i \xi_i^{(k)} \ (\underline{x}, t)$ is called an ensemble.

A random function, whose whole family of finite-dimensional distributions of probability are invariant under a displacement of time, is called a stationary random function (H. Cramer and M.R. Leadbetter, 1967). Random functions possessing the corresponding invariance in space are called homogeneous random functions.

The ensemble average, or the expectation of a random function, is defined as the integral of the product of this function with its finite-dimensional distributions of probability densities extended over the whole range of variations of the arguments of the function.

If the statistical characteristics of a stationary random process obtained by averaging a set of the realizations of this random process at a given time are, with a probability arbitrarily near unity, equal to the characteristics obtained by averaging a single realization for a sufficiently long interval of time, the process is said to be ergodic.

In practice, usually one realization is available and only the assumed ergodic characteristic allows the theoretical and experimental results to be compared, inasmuch as, in theory, ensemble averages are used, while, in practice, averages are determined in time. We shall denote ensemble averages by brackets $\langle\rangle$ and time averages by overbars.

2.1.1. Second Order Moments

In general, covariances, being the second order moments of random functions, are defined as

$$R_{ij}(\underline{x}, \underline{r}, t, \tau) = \langle (\xi_i(\underline{x}, t) - \langle \xi_i(\underline{x}, t) \rangle)(\xi_j(\underline{x}+\underline{r}, t+\tau) - \langle \xi_j(\underline{x}+\underline{r}, t+\tau) \rangle) \rangle ,$$

i.e. all correlations are defined with respect to different space-time points. Random functions possessing covariances are called second order random functions, and the properties which can be defined or determined by means of covariances are called second order properties. We shall always assume our random functions to be of second order and homogeneous in space and time, which is often called second order stationarity in the wide sense. For these functions the covariances have the form

$$R_{ij}(\underline{x}, \underline{r}, t, \tau) = R_{ij}(\underline{r}, \tau) .$$

2.1.2. Spectral Representation in Wave Number Space

The above definition of R_{ij} is often too general to be used in atmospheric physics. Either the covariances are defined with respect to different space points, the same time being used at both points, or the covariances are defined at a fixed space point and the time varies. The first case leads to a spectral decomposition of the corresponding random function in wave number space, the second case to a decomposition in frequency space.

Let us deal with a second order random function, $\underline{i}_i \xi_i(\underline{x})$, which is homogeneous in three spatial directions, and let us only consider correlations at the same time. The following theorem, the Wiener-Khintchine theorem, or rather an extension of the theorem established by H. Cramer (1940), is fundamental for the theory of spectral representation of random processes. The theorem may be stated as follows: to every homogeneous $\xi_i(\underline{x})$ there can be assigned a random process, $z_i(\underline{\kappa})$, with orthogonal increments, so that for each fixed $\underline{x}$ we have the spectral representation

$$\xi_i(\underline{x}) = \iiint_{-\infty}^{+\infty} e^{i\,\underline{\kappa}\,\cdot\,\underline{x}}\, dz_i(\underline{\kappa}) , \tag{2.1}$$

where $\underline{\kappa} \cdot \underline{x}$ denotes the inner product of the three-dimensional vectors $\underline{\kappa}$ and $\underline{x}$, i.e. $\underline{\kappa} \cdot \underline{x} = \kappa_1 x_1 + \kappa_2 x_2 + \kappa_3 x_3$. The random process $z_i(\underline{\kappa})$ is a process with orthogonal increments in the sense that

$\langle z_i(\underline{\kappa}) \rangle = 0$ for any three-dimensional interval

and

$$\langle dz_i(\underline{\kappa}') \, dz_j^*(\underline{\kappa}) \rangle = \begin{cases} 0 & \text{for any two disjoint three-dimensional intervals } \Delta\underline{\kappa}' \text{ and } \Delta\underline{\kappa} \\ dF_{ij}(\underline{\kappa}) & \text{otherwise.} \end{cases}$$

Here $z_j^*(\underline{\kappa})$ denotes the complex conjugate of $z_j(\underline{\kappa})$, and $F_{ij}(\underline{\kappa})$ is called the spectral distribution tensor.

The theorem further states that Eq. (2.1) holds good if, and only if, the correlation tensor can be represented as

$$R_{ij}(\underline{r}) = \iiint_{-\infty}^{\infty} e^{i\,\underline{\kappa}\,\cdot\,\underline{r}}\, dF_{ij}(\underline{\kappa}). \tag{2.2}$$

If the $R_{ij}(\underline{r})$ falls off sufficiently rapidly at infinity, this three-dimensional Fourier-Stieltjes integral can be written as an ordinary three-dimensional Fourier integral of the spectral density tensor

$$\Phi_{ij}(\kappa_1, \kappa_2, \kappa_3) = \frac{\partial^3 F_{ij}(\kappa_1, \kappa_2, \kappa_3)}{\partial\kappa_1\, \partial\kappa_2\, \partial\kappa_3} ,$$

and we have the Fourier transform pairs

$$\begin{aligned} R_{ij}(\underline{r}) &= \iiint_{-\infty}^{\infty} e^{i\,\underline{\kappa}\,\cdot\,\underline{r}}\, \Phi_{ij}(\underline{\kappa})\, d\underline{\kappa} \quad \text{and} \\ \Phi_{ij}(\underline{\kappa}) &= \frac{1}{(2\pi)^3} \iiint_{-\infty}^{\infty} e^{-i\,\underline{\kappa}\,\cdot\,\underline{r}}\, R_{ij}(\underline{r})\, d\underline{r} . \end{aligned} \tag{2.3}$$

Putting $\underline{r}$ equal to zero, we have

$$R_{ii}(0) = \langle \xi_i(\underline{x})\, \xi_i(\underline{x}) \rangle = \iiint_{-\infty}^{\infty} \Phi_{ii}(\underline{\kappa})\, d\underline{\kappa} . \tag{2.4}$$

Hence $\Phi_{ii}(\underline{\kappa})$ is the contribution to the variance (or kinetic energy) in the wave number range $\underline{\kappa}$ to $\underline{\kappa} + d\underline{\kappa}$.

Splitting R_{ij} up into an even and an odd part gives

$$R_{ij}(\underline{r}) = E_{ij}(\underline{r}) - O_{ij}(\underline{r}), \tag{2.5}$$

and taking the cosine and sine transforms, respectively, gives

$$\Phi_{ij}(\underline{\kappa}) = Co_{ij}(\underline{\kappa}) + i\, Q_{ij}(\underline{\kappa}) , \tag{2.6}$$

where the right-hand side contains the cospectral tensor and the quadrature spectral tensor respectively.

Putting $\underline{r}$ equal to zero we have

$$R_{ij}(0) = E_{ij}(0) = \langle \xi_i(\underline{x})\, \xi_j(\underline{x}) \rangle = \iiint_{-\infty}^{\infty} Co_{ij}(\underline{\kappa})\, d\underline{\kappa} , \tag{2.7}$$

which shows that the cospectral tensor measures the contribution to the covariance tensor in the wave number range $\underline{\kappa}$ to $\underline{\kappa} + d\underline{\kappa}$.

From the above, the following relations are valid

$$\begin{aligned} R_{ij}(\underline{r}) &= R_{ji}(-\underline{r}) \\ Co_{ij}(\underline{\kappa}) &= Co_{ij}(-\underline{\kappa}) = Co_{ji}(\underline{\kappa}) \\ Q_{ij}(\underline{\kappa}) &= -Q_{ij}(-\underline{\kappa}) = -Q_{ji}(\underline{\kappa}) . \end{aligned} \tag{2.8}$$

2.1.3. Spectral Representation in Frequency Space

However, the concepts in the foregoing section are still too general to be used in practice. Space spectra measured in the atmosphere are usually measured along a line, for instance a straight line parallel to the mean wind direction, or a circle of latitude. To obtain spectra that correspond to measurements, line-space spectra as well as time spectra, it should first be noted that the results we have given above are not restricted to a three-dimensional space; formally it is quite easy to extent the results to an n-dimensional random field in an n-dimensional space. While we still keep our random field three-dimensional, we now let $\underline{x}$ be a point in four-dimensional space.

$$\underline{x} = (x_1, x_2, x_3, t)$$

$$\underline{r} = \underline{x} - \underline{x}' = (x_1 - x_1', x_2 - x_2', x_3 - x_3', \tau), \quad \tau = t - t'$$

$$R_{ij}(\underline{x}, \underline{r}) = R_{ij}(\underline{r}) .$$

From Eq. (2.3) we generalize

$$R_{ij}(\underline{r}) = \iiiint_{-\infty}^{\infty} e^{i \underline{\kappa} \cdot \underline{r}} \Phi_{ij}(\underline{\kappa}) \, d\underline{\kappa} ,$$

$$\Phi_{ij}(\underline{\kappa}) = \frac{1}{(2\pi)^4} \iiiint_{-\infty}^{\infty} e^{-i \underline{\kappa} \cdot \underline{r}} R_{ij}(\underline{r}) \, d\underline{r} .$$

Let $\xi_i(\underline{x})$ be measured along the t-axis

$$R_{ij}(o,o,o,\tau) = \iiiint_{-\infty}^{\infty} e^{i \kappa_4 \tau} \Phi_{ij}(\underline{\kappa}) \, d\underline{\kappa}$$

$$= \int_{-\infty}^{\infty} e^{i \kappa_4 \tau} \, d\kappa_4 \iiint_{-\infty}^{\infty} \Phi_{ij}(\underline{\kappa}) \, d\kappa_1 \, d\kappa_2 \, d\kappa_3 .$$

Defining

$$\iiint_{-\infty}^{\infty} \Phi_{ij}(\underline{\kappa}) \, d\kappa_1 \, d\kappa_2 \, d\kappa_3 = S_{ij}(\kappa_4) \text{ say, we obtain}$$

$$R_{ij}(\tau) = \int_{-\infty}^{\infty} e^{i \kappa_4 \tau} S_{ij}(\kappa_4) \, d\kappa_4 ,$$

$$S_{ij}(\kappa_4) = \frac{1}{2\pi} \int_{-\infty}^{\infty} e^{-i \kappa_4 \tau} R_{ij}(\tau) \, d\tau . \tag{2.9}$$

$S_{ij}(\kappa_4)$ is the time spectral tensor and $\kappa_4 = \omega$ is usually called the frequency and the wavelength is called the period T. Just as before we can split the complex $S_{ij}(\omega)$ up into a sum of a cospectral tensor $Co_{ij}(\omega)$ and a quadrature spectral tensor $Q_{ij}(\omega)$ and with relations similar to those of Eq. (2.8):

$$\begin{aligned} Co_{ij}(\omega) &= Co_{ij}(-\omega) = Co_{ji}(\omega), \\ Q_{ij}(\omega) &= -Q_{ij}(-\omega) = -Q_{ji}(\omega) . \end{aligned} \tag{2.10}$$

2.1.4. The One-Dimensional Wave Number Spectrum-Tensor

Let $\xi_i(\underline{x})$ be measured along the x_1-axis

$$R_{ij}(r_1,o,o,o) = \iiiint_{-\infty}^{\infty} e^{i \kappa_1 r_1} \Phi_{ij}(\underline{\kappa}) \, d\underline{\kappa}$$

$$= \int_{-\infty}^{\infty} e^{i \kappa_1 r_1} \, d\kappa_1 \iiint_{-\infty}^{\infty} \Phi_{ij}(\underline{\kappa}) \, d\kappa_2 \, d\kappa_3 \, d\kappa_4 .$$

$\iiint_{-\infty}^{\infty} \Phi_{ij}(\underline{\kappa}) \, d\kappa_2 \, d\kappa_3 \, d\kappa_4 = G_{ij}(\kappa_1)$, we obtain

$$R_{ij}(r_1) = \int_{-\infty}^{\infty} e^{i \kappa_1 r_1} G_{ij}(\kappa_1) \, d\kappa_1 ,$$

$$G_{ij}(\kappa_1) = \frac{1}{2\pi} \int_{-\infty}^{\infty} e^{-i \kappa_1 r_1} R_{ij}(r_1) \, dr_1 .$$

$G_{ij}(\kappa_1)$ is the one-dimensional wave number spectral tensor.

2.2. The Eddy Concept

Turbulent flow is normally thought of as a superposition of many eddies of varying sizes and orientations occurring more or less at random throughout the fluid. In describing an eddy, we think of a circulating region of fluid of some characteristic size, isolated or closely connected with a number of other eddies. It is obvious that the relation between kinetic energy and eddy size is most precisely defined by the spatial Fourier transform $\Phi_{ij}(\underline{\kappa})$, Eq. (2.3).

Introducing spherical coordinates in $\underline{\kappa}$-space and integrating over the angle variables, we obtain the integrated spectrum $\Psi_{ij}(\kappa)$ averaged over directions:

$$\kappa_1 = \kappa \sin\theta \cos\phi ,$$

$$\kappa_2 = \kappa \sin\theta \sin\phi ,$$

$$\kappa_3 = \kappa \cos\theta ,$$

$$\Psi_{ij}(\kappa) = \int_0^{\pi} \int_0^{2\pi} \kappa^2 \Phi_{ij}(k,\theta,\phi) \sin\theta \, d\phi \, d\theta .$$

Furthermore, it is convenient to consider only a scalar quantity rather than a tensor quantity. The most natural scalar to consider is the trace of $\Psi_{ij}(\kappa)$. Thus, in speaking of eddy size and kinetic energy, attention is often confined to the so-called three-dimensional scalar energy-spectrum

$$\Psi_{ii}(\kappa) = \int_0^{\pi} \int_0^{2\pi} \kappa^2 \Phi_{ii}(k,\theta,\phi) \sin\theta \, d\phi \, d\theta ,$$

and from Eq. (2.4) the relation between kinetic energy density $\propto \langle u_i(\underline{x}) u_i(\underline{x}) \rangle$ and $\Psi_{ii}(\kappa)$ is:

$$\langle u_i(\underline{x}) u_i(\underline{x}) \rangle = \int_0^{\infty} \Psi_{ii}(\kappa) \, d\kappa .$$

Having estimated $\Psi_{ii}(\kappa)$ from data, is it then possible from $\Psi_{ii}(\kappa)$ to estimate the distribution of the eddy size in the flow? To shed some light on this problem let us follow an example given by Townsend (1956), and think of an isolated eddy as represented by the velocity field

$$u_1 = a^2 x_2 \exp(-\tfrac{1}{2} a^2 (x_1^2 + x_2^2 + x_3^2)) ,$$

$$u_2 = -a^2 x_1 \exp(-\tfrac{1}{2} a^2 (x_1^2 + x_2^2 + x_3^2)) ,$$

$$u_3 = 0 .$$

The form of the velocity field indicates that the eddy has a characteristic size $1/a$.

Assuming the eddies to be homogeneously superimposed at random with average separation between centres $\gg 1/a$, Townsend found

$$\Psi_{ii}(\kappa) = 2\pi A \kappa^4 \exp(-\kappa^2/a^2) ,$$

where A is a constant. $\Psi_{ii}(\kappa)$ has maximum at $\kappa = a\sqrt{2}$ and most of $\Psi_{ii}(\kappa)$ is concentrated near this value. We shall assume that we can neglect the spread in $\Psi_{ii}(\kappa)$ around $\kappa = a\sqrt{2}$, and say that when many different eddy sizes are present, the number of eddies with sizes equal to $1/\kappa$ is simply proportional to $\Psi_{ii}(\kappa)$. Still, what we are able to measure are one-dimensional wave number tensors, for instance $G_{ij}(\kappa_1)$, and only when strong symmetry conditions are imposed on the flow is there a simple relation between $\Psi_{ii}(\kappa)$ and $G_{ii}(\kappa_1)$. Despite this, we shall discuss measured $G_{ii}(\kappa_1)$ in terms of characteristic eddy dimensions.

2.3. Taylor's Hypothesis

As to the manner of observation, data covering different scales near the ground generally exist in the form of time series, so usually we have no direct knowledge of the spatial structure of the velocity field. To estimate spatial structure from temporal data, a hypothesis advanced by Taylor (1938) is normally used. He suggested that when the turbulence level is low enough, the evolution in spatial pattern of a lump of fluid during its transit past a fixed point may be so slight that the pattern is effectively 'frozen' during passage. Then the changes at the point with time are due only to spatial non-uniformities being convected past the point at mean wind speed.

In spectral space we can use Taylor's hypothesis to give an approximative relation between a frequency spectrum, for instance $S_{11}(\omega)$ and a one-dimensional wave number spectrum $F_{11}(\kappa_1)$, consisting of replacing the measured frequency ω by $\kappa_1 \bar{u}$, where $\bar{u} = \langle u_1(t) \rangle$, so that $\omega S_{11}(\omega) = (\omega/\bar{u}) F_{11}(\omega/\bar{u})$.

Experimental evidence, Monin and Yaglom (1971), shows that Taylor's hypothesis holds for scales up to ~1 km in the planetary boundary layer. On larger scales the speed of the eddies is not constant but depends on the size of the eddies, and a relation between frequency and space spectra requires a knowledge of the dependence of energy propagation on scale. Since waves in the atmosphere in general are dispersive, individual waves in the system move at a speed (C) different from that of the energy. The energy-carrying velocity or the group velocity (C_g) can be related to wave velocities and scales by

$$C_g = C + \kappa \frac{\partial C}{\partial \kappa} .$$

In order to compare frequency and spatial spectra for large scales, C_g rather than C should be used in Taylor's hypothesis. Some evidence of this has been given by Vinnichenko (1970). Unfortunately direct measurements of C_g are not available, and we have to use the mean wind speed in Taylor's hypothesis knowing the results to be rather dubious as we approach small wave numbers. For instance, it takes a synoptic pressure system with radius ~3000 km several days to pass a fixed point, a period comparable with the lifetime of the system.

2.4. The Limits of Atmospheric Spectra

Space spectra are bounded both in the direction of large wave numbers and in the direction of small wave numbers.

$\lambda_{\text{minimum}} \approx (\nu^3/\varepsilon)^{1/4}$, the micro-scale of turbulence
$\approx$ 0.1 cm (Batchelor, 1959)

where ν and ε are the viscosity and dissipation parameters.

$\lambda_{\text{maximum}} \langle$ 40,000 km, the length of the equator.

The corresponding periods in the frequency spectrum, using Taylor's hypothesis, are

$T_{(\lambda \text{ min})} \sim 10^{-4}$ sec

$T_{(\lambda \text{ max})} \sim 1$ month ,

which shows that the frequency spectrum must be bounded in the direction of high frequencies, and for periods greater than ~1 month it is impossible to associate time spectra with space spectra. Frequency spectra are not bounded in the low frequency end, indeed oscillations of meteorological parameters are found with periods ranging from a fraction of a second to thousands of years, as indicated on figs. 1 and 2: The frequency spectra of the two atmospheric scalars, temperature and horizontal wind speed.

2.5. The Graphical Representation of Spectra

The wind speed spectrum, fig. 2, is presented in an invariant form often used in meteorology where a range of frequencies extending over several decades is not uncommon. We have

$$\langle \xi^2 \rangle = 2 \int_0^\infty S(\omega)\, d\omega = 2 \int_0^\infty \omega S(\omega)\, d \ln \omega ,$$

i.e., we plot $\omega S(\omega)$ versus $\ln \omega$. The invariance can be derived from the following reasoning, (Dutton, 1971):

$$\tfrac{1}{2} \langle \xi^2 \rangle = \int_0^\infty S(\omega)\, d\omega = \int_0^\infty a S(a\eta)\, d\eta ,$$

where η is a new variable $\omega = a\eta$, $d\omega = a\, d\eta$ and a is a constant. The energy density associated with variable η is

$$S'(\eta) = a S(a\eta) ,$$

which gives

$$\eta S'(\eta) = \eta a S(a\eta) = \omega S(\omega) ,$$

so that the spectral form $\eta S'(\eta)$ is identical with $\omega S(\omega)$. In the region where Taylor's hypothesis applies we have

$$\omega S(\omega) = \kappa S'(\kappa)$$

and $\omega = \bar{u} \kappa$.

Fig. 2 shows a log-linear version where $\omega S(\omega)$ is plotted versus $\log_{10} \omega$, i.e.

$$\tfrac{1}{2} \langle \xi^2 \rangle = \int_0^\infty \omega S(\omega)\, d \ln \omega = \ln 10 \int_0^\infty \omega S(\omega)\, d \log_{10} \omega .$$

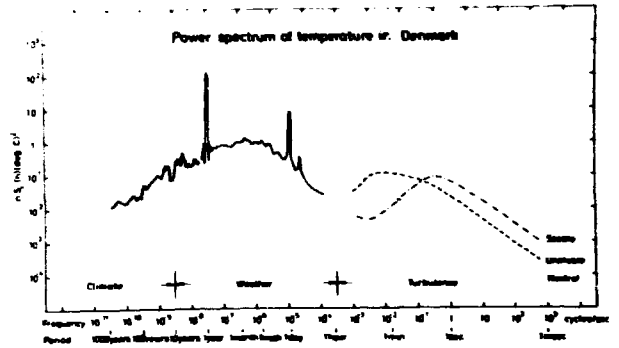

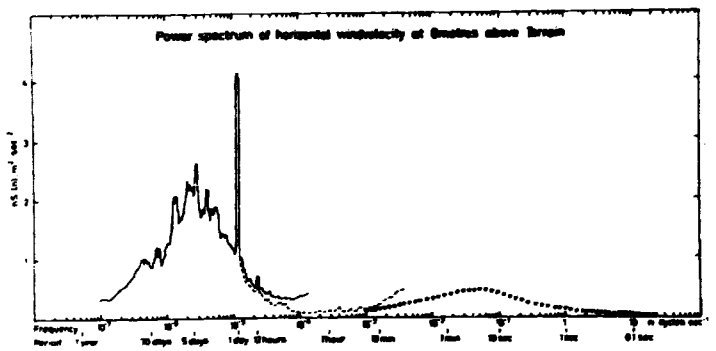

Fig. 1. Top. Power spectrum of temperature (from an investigation by E. L. Petersen and S. E. Larsen, 1973. To be published). ∞ Yearly averages of the O^{18}/O^{16}-ratio in precipitation 1174-1966. The data are from an ice-core from Greenland (S. J. Johnsen, et al., (1972)) and calibrated against a two hundred years' temperature record from Southern Germany. – Hourly measurements of ten-minute averages taken at Risø 1958-1967 at 6 m height. The high frequency parts are based on measurements from Kansas 1968 (N. E. Busch and S. E. Larsen, 1972) for three different cases of atmospheric stability. – . – . – z/L = -0.5; ..... z/L = -0.02; – – – z/L = 0.5.

Fig. 2. Bottom. Power spectra of the horizontal wind speed at 7 m above the ground. —— Hourly measurements of ten-minute averages taken at Risø 1958-1967; – – – One-minute averages measured at two-minute intervals at Risø during five weeks in 1971. The high frequency parts of the two spectra are influenced by aliasing. ..... Turbulence spectrum measured in Kansas 1968 (N. E. Busch and S. E. Larsen, 1972), based on analogue analysis of twenty-five hourly records.

The temperature spectra fig. 1 is presented in a log-log plot, a representation used when both the range of frequencies and the range of spectral values extend over several decades. This representation has the advantage of presenting constant powers of frequency as straight lines with a slope corresponding to the powers, but it is not area preserving as is the log-linear representation.

2.6. Reynold's Convention

The most important, and at the same time the simplest statistical characteristics of random fields of atmospheric parameters are their mean values $\langle \underline{i}_i \xi_i(\underline{x}) \rangle$. The differences $\underline{i}_i \xi_i'(\underline{x}) = \underline{i}_i \xi_i(\underline{x}) - \langle \underline{i}_i \xi_i(\underline{x}) \rangle$ between individual values of the field $\underline{i}_i \xi_i(\underline{x})$, and its mean values are called the fluctuations of the field. This decomposition of the parameters into mean values and fluctuations is called the Reynold's convention and plays a fundamental role in all investigations of random fields in fluid dynamics.

Time series of meterological parameters often prove to include some periodic functions of time, commonly with periods of a day and a year, and we shall thus consider our meteorological parameters measured in the time domain as consisting of a climatological mean and one or more periodic components of fixed phase angles, and a deviation which is considered to be a stationary random function. Unfortunately, the last point is a crude approximation, since in most cases with non-stationary means, the fluctuations are not stationary functions, but no really feasible methods are available in spectral analysis of periodic random functions so one must draw heavily on the assumption of stationarity.

The daily and yearly periodicities in the parameters will be subject to a thorough analysis in chapter 7, and although we shall not deal much with the concept of climate and climate oscillations, it is worth noting from fig. 1 that there are oscillations of temperature with periods of many tens of years.

Summing up we write:

$$\xi_i(x_1,x_2,x_3,t) = \langle \xi_i(x_1,x_2,x_3,t) \rangle + \xi_i'(x_1,x_2,x_3,t)$$

$$\langle \xi_i(x_1,x_2,x_3,t) \rangle = \langle \xi_i(x_1,x_2,x_3) \rangle + \langle \xi_i''(x_1,x_2,x_3,t) \rangle$$

$\langle \xi_i(x_1,x_2,x_3) \rangle = \xi_i^c(x_1,x_2,x_3)$ the climatological mean

$\langle \xi_i''(x_1,x_2,x_3,t) \rangle = \xi_i^p(x_1,x_2,x_3,t)$ the periodic mean

$\xi_i'(x_1,x_2,x_3,t)$ the fluctuating component where

$\langle \xi_i'(x_1,x_2,x_3,t) \rangle \equiv 0$.

3. THE DATA RECORDS

3.1. Introduction

The spectra presented in this report are, with minor exceptions, based on measurements of meteorological parameters at Risø, Karlstrup and Station Nord, the two first on Zealand and the last in northern Greenland. All the parameters are measured as functions of time. Tables 1a - 1d contain information about the stations, the records, and the calculated spectra.

3.2. The Risø Records

The Risø 125 m meteorological tower is situated on a narrow peninsula, surrounded by bays of varying size (see fig. 3). The foundation of the tower is on a slope at a height of 6.5 m above mean sea level. The tower is composed of fifteen 8 m-long sections bolted together. In cross section the sections present an equilateral triangle with 1.76 m-long sides. The three sides face north, south-west, and south-east. The instruments were mounted on triangular booms extending from the south-west side of the tower and were positioned 2.35 m from the lattice work of the tower.

Wind speeds were measured at 7 heights above the base of the tower: 7, 23, 39, 56, 72, 96, and 123 m; temperatures at the same heights and at 2 m; wind directions at 7, 56, and 123 m; moisture at 2 and 123 m. Wind speeds and directions were obtained from cup anemometers and vanes, temperatures were sensed by platinum resistance thermometers, and humidity by lithium chloride humidiometers. All measurements were recorded on strip-charts. The types of instruments have been subject to changes throughout the years, and instruments have been interchanged between heights. Great care has been taken by the Risø personnel in daily maintenance to keep the measurements at their best. Further information on the site, the instruments, and recording system is given elsewhere.

From the strip-charts ten-minute average winds, wind directions, temperatures and humidities centred on every hour were evaluated, punched on cards, and transferred to magnetic tape for the 10-year period 1958-1967. The wind speeds were evaluated to the nearest half metre per second for the period 1958-1963, thereafter to the nearest tenth of a metre per second. The wind directions were evaluated in sectors of 10 degrees (0-360 degrees are used), and temperature to the nearest tenth of a degree centigrade.

An analysis of the wind profiles (H. A. Panofsky and E. L. Petersen, 1972) revealed a characteristic variation of wind with height depending on wind directions, i. e. on the character of the up-stream surface. Thus a single discontinuity in surface roughness shows up as a single "kink" in the wind profile and a double discontinuity as a double kink (see fig. 3).

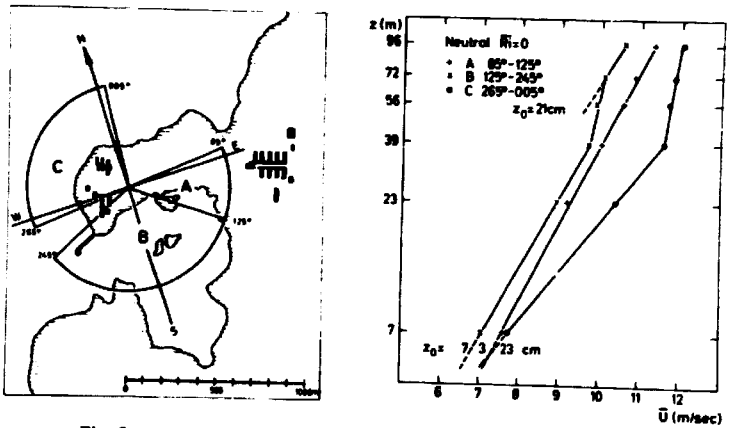

Fig. 3. Mean wind profiles for hydrostatically neutral air, measured at Risø with the wind coming from different angular sectors as shown on the map of Risø. The surface roughness changes are clearly reflected by "kinks" in the profiles, the characteristics of which depend on the wind direction.

It was shown that the height of a single kink and the height of the lowest kink were in good agreement with theory. It was demonstrated that the roughness lengths computed for the immediate surrounding of the tower vary with wind directions in a manner consistent with terrain features, and further that the mean profile obtained when the trajectory passes over relatively homogeneous terrain is represented quite well by wind profile expressions that are usually only applied to the surface layer.

E. L. Petersen and P. A. Taylor (1973) compared the profiles observed in near-neutral conditions and those predicted using models based on mixing-length theory (P. A. Taylor, 1969) and the turbulent energy equation (E. W. Peterson, 1969). The comparisons appeared to be moderately good, but some features of the observed profiles were missing from the theoretical predictions (see fig. 4).

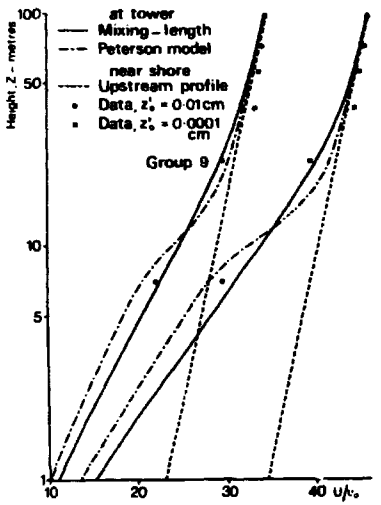

Fig. 4. Computed and observed wind profiles for hydrostatically neutral air with a single discontinuity in the surface roughness. The roughness length for the water z'_o, determined from the observed profile, is unrealistically small, therefore two reasonable values are used for comparison purposes.

In addition to the tower measurements, a record of wind speed was obtained during the month of December 1971. Here use was made of a fast responding cup anemometer placed at a height of 6 m on top of a building close to the tower. The data were automatically compiled by a digital magnetic tape recorder after some low pass filtering, and the final record consists essentially of one-minute average wind speed block averaged over the last half of consecutive two-minute periods.

3.3. The Karlstrup Record

During the summer of 1972 the meteorology section participated in a diffusion experiment managed by the Environmental Technology Division of the Danish company, F. L. Smidth and Co. A/S. The experiment was carried

out near one of the company's large concrete manufacturing plants, Karlstrupværket, 3 km west of the Øresund coast in a very flat area. The section measured wind speed, wind direction, and temperature. The sensors were mounted on top of a 2 m mast, and for practical reasons the mast was placed on top of a small hill; the total height of the sensors was 12 m above mean sea level.

Wind speeds and wind directions were obtained with fast responding cup anemometers and vanes, and temperatures were sensed by platinum resistance thermometers. For consecutive 2-minute periods nine point measurements were taken with non-equidistant time spacing: viz. four wind speeds, three wind directions, and two temperatures. The data were automatically compiles by a digital magnetic tape recorder.

3.4. The Station Nord Record

In the summer of 1972 an automatic climatological recording system was installed at the Danish airport Nord in north-east Greenland by staff of the Danish Meteorological Institute together with staff of the Meteorology Section of the Danish AEC (L. Kristensen and J. Taagholt, 1973). The station is situated at an elevation of 36 m in a flat, homogeneous terrain. Wind speed and wind direction were obtained from a cup anemometer and a wind vane both located 5.3 m above the ground on top of a steel pipe. Other parameters measured were air temperature and pressure. The recording takes place every hour, the sampling system being the same as for the two other records. The wind speed recorded is a block average over an hour, whereas the direction is an instantaneous measurement.

Table 1 a

Station	Elevation (m)	Speed U-comp V-comp	Date	Sampling duration	Geograph. position	Averaging time
Risø 1	7	S U V	1 Feb. 1958- 31 Dec. 1967	10 years	55° 41' N 12° 05' E	10 min. centered around every hour
	23	S				
	39	S				
	56	S U V				
	72	S				
	96	S				
	123	S U V				
Risø 2	6	S	21 Dec. 1971- 27 Dec. 1971	6 days	55° 41' N 12° 05' E	1 min. every 2nd min.
	6	S	27 Dec. 1971- 3 Jan. 1972	7 days		
Karlstrup	1	U V	27 May 1972- 8 July 1972	42 days	55° 33' N 12° 13' E	2 min.
Station Nord	6	S U V	12 June 1972- 19 Aug. 1972	69 days	81° 36' N 16° 40' W	1 hour

Table 1 b

Station series	Fig.	Page	Type of spectr.	Period	No. of realizations	No. of data-points in one realization	No. of estimates after smoothing	Confid. lim.	μ m/sec.	e^2 m^2/sec^2	Smoothing parameters b	a	c
Risø 1 7 m	11 (1, 6)		S	10 years	5	16384	3505	+	5.0	7.9	0.1	0.02	10
	21		S		5	16384	56		5.0	7.9	0.2	0.5	15
	21		U V U+V		20	4096	55		0.6 0.8 1.0	16.6 14.4 21.0	0.2	0.5	5
Risø 1 23 m	12		S	10 years	5	16384	3505		6.1	10.1	0.1	0.02	10
39 m	13								6.8	11.5			
72 m	15								7.4	12.7			
96 m	16								7.7	13.1			

Table 1 c

Station series	Fig.	Page	Type of spectr.	Period	No. of realizations	No. of data-points in one realization	No. of estimates after smoothing	Confid. lim.	μ m/sec.	σ^2 m^2/sec^2	Smoothing parameters b	a	c
Risø 1	14		S	10 years	5	16384	3505	+	7.1	12.1	0.1	0.02	10
56 m	22		S		5	16384	56		7.1	12.1	0.2	0.5	15
	22		U						1.2	33.5			
	22		V		20	4096	55		1.0	24.0	0.2	0.5	5
	22		U+V						1.6	57.5			
	25		Q					+					
	27		2fQ/ωS		20	4096	23				0.5	0.5	10
Risø 1	17		S	10 years	5	16384	3505		8.2	12.6	0.1	0.02	10
123 m			S		5	16384	56		8.2	12.6	0.2	0.5	15
			U						0.5	40.5			
			V		20	4096	55		1.25	26.9	0.2	0.5	5
			U+V						1.3	67.4			

Table 1 d

Station series	Fig.	Page	Type of spectr.	Period	No. of realizations	No. of data-points in one realization	No. of estimates after smoothing	Confid. lim.	μ m/sec	σ^2 m^2/sec^2	Smoothing parameters b	a	c
Risø 2	7		S	1 week	1	4096	1862	+	5.0	5.5	0.1	0.01	10
6 m	8		S		1	4096	1862	+	5.2	6.1	0.1	0.01	10
Karlstrup	9		U+V	42 days	1	32768	647		0.6	4.2	0.1	0.1	5
Station Nord	10		S	69 days	3	512	243	+	4.3	7.8	0.05	0.05	2
	24		U				198		-0.3	9.1	0.1	0.1	2
	24		V				198		-1.0	15.9	0.1	0.1	2
	24		U+V				198		1.0	25.0	0.1	0.1	2
	26		Q				243	+			0.05	0.05	2
	28		2fQ/ωS				198				0.1	0.1	2

4. PRACTICAL SPECTRAL ANALYSIS

4.1. The FFT

The time series considered in this report are all discretely sampled hence digital analysis techniques are to be applied. An algorithm for the computation of Fourier transforms, that requires much less computational effort than former conventional methods has been reported by Cooley and Tukey (1965). A whole issue of the IEEE Transactions on Audio and Electroacoustics (1967) was devoted to the method and today it is almost the only method used to calculate discrete Fourier transforms.

The algorithms, commonly called Fast Fourier Transforms, are available in computer software packages and are all very fast and accurate and can operate in just the space required to store the original data.

4.2. The Discrete Fourier Transform

The mathematical basis of the method are the formulas

$$y_i(l) = \sum_{k=0}^{n-1} \hat{y}_i(k) \exp(-2\pi i l k/n) \qquad (4.1)$$

$$\hat{y}_i(k) = \frac{1}{n} \sum_{l=0}^{n-1} y_i(l) \exp(2\pi i l k/n)$$

$$F_{ij}(k) = \hat{y}_i(k)\, \hat{y}_j(k)^*,$$

where

$$y_i(l) = y_i(t_l)$$

are discretely sampled time series,

$$\hat{y}_i(k) = \hat{y}_i(k \Delta \omega)$$

the discrete Fourier transforms of $y_i(l)$, and

$$F_{ij}(k) = F_{ij}(k \Delta \omega)$$

the digital estimate of the true spectrum, l and k being respectively a discrete measure of time and a discrete measure of frequency ω (cyclee per unit time).

Let T_o denote the record length, n the total number of data points, Δt the sampling interval, and l an integer bound to the interval $0 \leq l \leq n-1$. Then we have the relations:

recording time $t_l = l \Delta t$
record length $T_o = n \Delta t$

frequency $\omega_k = k$
elementary frequency $\Delta\omega = 1/T_o$
lowest possible frequency $= \Delta\omega = 1/T_o$
highest possible frequency (the Nyquist frequency) $= 1/(2\Delta t)$

A complex FFT-procedure implemented on Risø's Burroughs B6700 was used for all our spectral calculations. The procedure has the effect of transforming a complex vector y(l), the dimension of which must be a power of two, into its Fourier transform. It can be shown (see e.g. C. Bingham et al., (1967), L. Kristensen and C. Paulson, (1970)) that it is possible to use this procedure to calculate the power spectra, the cospectrum, and the quadrature spectrum of two parallel time series $y_i(l)$ and $y_j(l)$, if y(l) is stored as

$$y(l) = y_i(l) + i\, y_j(l).$$

4.3. Problems in Digital Spectral Analysis

In practical spectral analysis certain problems arise as to how to determine the degree of resemblance of the computed spectra to the true spectra. An exhaustive treatment of these problems, such as aliasing, effects of non-stationarity, choice of record length and sampling interval, and the statistical reliability of the results, can be found in the literature (J. L. Lumley and H. A. Panofsky, 1964, E. J. Hannan, 1970, L. Kristensen, 1971).

A number of decisions must be made, and it is of extreme importance that these decisions reflect some prior knowledge of the nature of the spectra i.e. it should be possible from the physical process under consideration to estimate special bandwidths (frequency-intervals) where it is expected to find a high concentration of spectral mass, to estimate lines in the spectrum connected with true periodicities, and to estimate the rate of decrease of the spectrum for increasing ω and for ω being greater than some ω'.

The choice of Δt and T_o reflects a compromise between a demand for a representative record, a high degree of time and spectral resolution meaning T_o large and Δt small, and the limits set up by the measuring and recording devices.

If the record length, T_o, exceeds the working store of the computer it is necessary to divide the record into N pieces of length T and the average the spectral estimates over these pieces. But nothing is gained by subdividing the record, except a saving of computer time; on the contrary,

the longer T is compared to the integral scale, i.e. the memory of the process, the better justified is the assumption of ergodicity.

Increasing T means narrowing $\Delta\omega$ and a higher spectral resolution is thus given, but this is paid for by a lower statistical confidence.

4.4. Smoothing

In order to improve the statistical confidence of the spectral estimates, it is necessary to smooth the raw spectral estimates, $F_{ij}(\omega_k)$, over frequency intervals:

$$G_{ij}(\omega_o) = \frac{1}{\Delta\omega} \int_{\omega_o - \Delta\omega/2}^{\omega_o + \Delta\omega/2} F_{ij}(\omega)\, d\omega, \qquad (4.2)$$

where $G_{ij}(\omega_o)$ are the smoothed spectral estimates.

The smoothing procedure we have used is essentially smoothing by running block averaging over bands of constant relative bandwidth, i.e. the spectral estimates and corresponding frequencies are averaged over frequency intervals, $\Delta\omega$, where the relative bandwidth

$$b = \Delta\omega/\omega_o \qquad (4.3)$$

equals a constant. Adjacent frequency intervals have a non-overlapping interval, $a\Delta\omega$, where $a < 1$ is a constant, i.e.

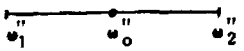

$$\omega'_2 = \omega'_1 (1+b)$$

$$\omega''_1 = \omega'_1 + a(\omega'_2 - \omega'_1) = \omega'_1 (1 + ab)$$

$$\omega''_2 = \omega''_1 (1+b),$$

hence

$$\frac{\omega''_o}{\omega'_o} = \frac{1/2\,(\omega''_2 + \omega''_1)}{1/2\,(\omega'_2 + \omega'_1)} = \frac{\omega''_1\,(2+b)}{\omega'_1\,(2+b)} = \frac{\omega'_1\,(1+ab)}{\omega'_1}$$

$$\frac{\omega''_o}{\omega'_o} = 1 + ab = \text{constant} \qquad (4.4)$$

Because the spectra are discrete it is not possible to satisfy Eqs. (4.3) and (4.4) at the low frequency end. We have chosen to demand a minimum number

$C > 1$, of estimates to be contained in one interval, and to let $\Delta\omega/\omega_o \to b$ asymptotically in a hyperbolic fashion

$$\Delta\omega = \sqrt{(C/T)^2 + (\omega_o b)^2}\,.$$

The standard deviation divided by the square root of the total number of estimates used in computing each smoothed estimate is taken as a measure of confidence. The justification of this is that the distribution of the spectral estimates is the distribution of a variance, hence a chi-square distribution. Choosing the smoothing parameters so that the number of smoothed estimates in each interval is large, we can replace the chi-square distribution by a normal distribution, the error performed being largest for low frequency estimates.

In this report spectra with confidence limits are represented in the form

$\omega(G_{ij}(\omega) \pm$ the standard deviation of $G_{ij}(\omega))$ versus $\log_{10}\omega$.

This interval is then a 68% confidence interval for ω greater than some ω_M.

4.5. Missing Observations

Abortive attempts were made to investigate how different methods for replacing missing data affect the spectra. The experience we gained showed that the spectra exhibit a remarkable indifference to the different methods, a feature commonly observed, see e.g. R. Thompson (1971).

Thus in the calculations of scalar spectra we have simply replaced missing observations by estimated mean values, and in the calculations of vector component spectra we let the components retain their last calculated values through the periods without measurements of either magnitude or direction. The influence of missing observations is of course greatest for the component spectra; in the Risø tower series, 15% of the combined measurements of speed and direction lacks at the top, 13% at 56 m, and 12% at 7 m. Despite this there is an almost curiously good agreement between the spectra from the three heights, so we have good confidence in them for an order of magnitude.

A technique to replace missing observations is indicated by N. E. Busch and E. L. Petersen (1971). The technique is founded on the Karhunen-Loeve theorem (Loeve, 1955) and uses a representation of realizations, one realiz-

action e.g. being one day's measurement of temperature, in terms of so-called proper or empirical orthogonal expansions.

Although the method was found to be very promising, lack of time prevented us from using it in this study.

5. SPECTRA OF THE HORIZONTAL WIND VECTOR

5.1. Introduction

All our data records pertain to the lowest 100 m of the atmosphere. But since large-scale motion is essentially two-dimensional, no basic difference in the horizontal scales of perturbations in the wind field will appear in the lowest 5000 m, except that the amplitudes may change with height and that smaller scales connected with the prevailing three-dimensional motion are superimposed near the ground. Fig. 5 shows schematically the main groups of scales of the atmospheric system: microscale, mesoscale, and synoptic scale.

5.2. Composite Spectra

Up till now the only feasible method to estimate spectra over large ranges of periods is to patch together individual spectra computed separately over smaller ranges.

A composite spectrum of the horizontal wind speed as estimated from three different time series was given in fig. 2. It is of course a very dubious precedure to patch together individual spectra so that different portions of the combined spectra do not refer to the same record and, as far as fig. 2 is concerned, not even to the same geographical location. Interpretation is in fact difficult. Fortunately, all published spectra of wind speed covering long ranges of periods substantiate the same features: a large contribution to the variance at macroscale, a deep minimum at mesoscale, and a more or less weak maximum in the microscale. Fig. 6 shows three composite spectra. The top one is the now classic Van der Hoven Spectrum, calculated in 8 overlapping frequency intervals using data from the three levels 31, 108, and 125 m at the meteorological tower of Brookhaven National Laboratory (Van der Hoven, 1957). The spectrum at the bottom is calculated by F. Fiedler (1971) using data obtained at a height of 50 m near Munich covering 3 frequency intervals. The Risø spectrum from fig. 2 is shown here for comparison purposes. These three spectra, in contrast to all other spectra in this report, have been multiplied by a factor of two in order to let the

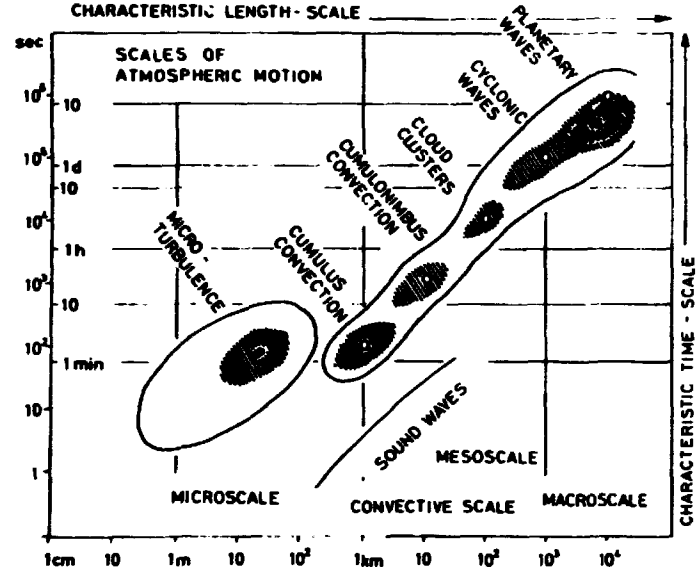

Fig. 5. Scale of atmospheric motion (after H. Fortak, 1971). Macroscale or synoptic scale motion includes all scales of motion that can be analyzed on the basis of weather maps. These motions are quasi-two-dimensional. In microscale systems the vertical and horizontal velocities are of the same order of magnitude. Mesoscale occurs between microscale and synoptic scale; it includes systems with strong diurnal variations such as sea breezes, mountain-valley flow and the low-level jet. It also includes frontal structures, squall lines and long gravity waves (F. Fiedler and H.A. Panofsky, 1970).

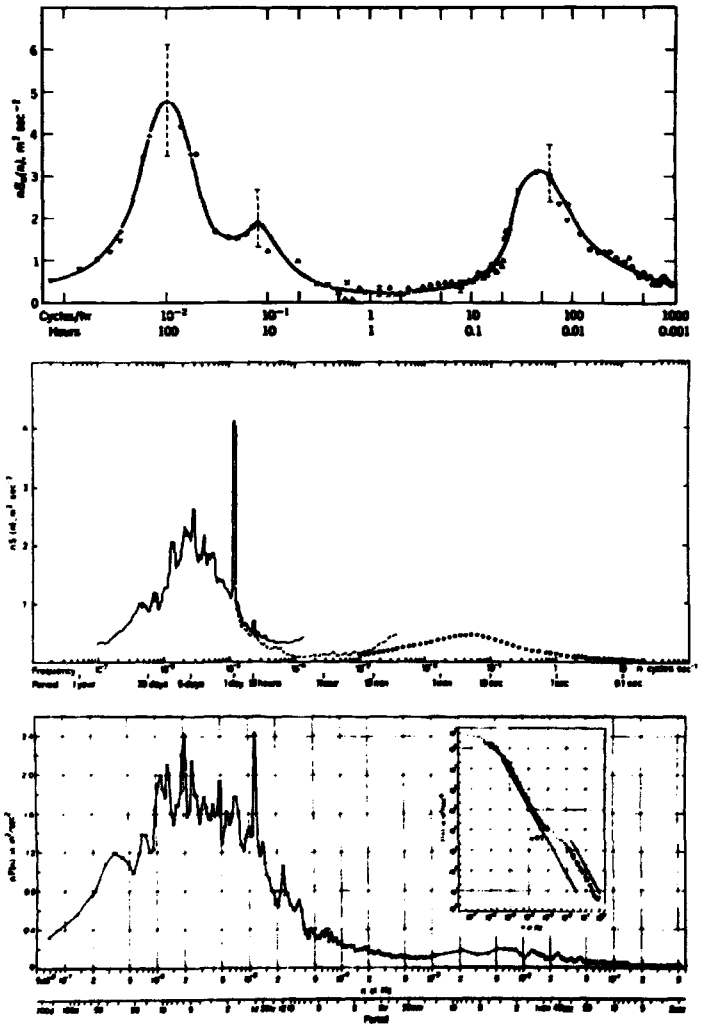

Fig. 6. Three composite spectra of the horizontal wind speed measured from top to bottom at: Brookhaven, U.S.A. (Van der Hoven, 1967); Risø, Denmark; Munich, Germany (F. Fiedler, 1971). The heights are 100, 8, and 50 m respectively.

variance of the corresponding time series be given by the area under the spectrum.

5.2.1. The Spectral Gap

The first important feature of the three spectra to be noticed is that they all have a wide mesometeorological minimum region with periods from one day to about 10 minutes. A general existence of this gap is very important to prove, if possible, in the discussion of the predictability of the atmospheric motions and of the parameterization of small scale motions in terms of the characteristics of large scale motions on the other side of such a gap (F. Fiedler and H.A. Panofsky, 1970). Parameterization means a simplification introduced into a dynamical model by preassigning the magnitude of a physical effect rather than by allowing the effect to be realistically determined internally as a consequence of the dynamics of the system.

Of course, the problem of the interaction between synoptic and microscale motions can be viewed in another way. One might seek a complete physical understanding of the mechanisms by which the scale interactions take place (recommended by F. P. Bretherton et al. 1969: ---" it appears that the existence or non-existence of a spectral gap is of small importance for many processes. A search for the detailed physics of atmospheric processes is more important than, and to a great extent independent of, a search for a spectral gap"). This is the approach of the physical scientist who is interested in turbulence for its own sake, but if one wants to study the interactions on all scales in the atmosphere, and no gap exists, then it would be necessary to study all these scales simultaneously. Fortunately, from various studies (H. A. Panofsky and Van der Hoven, 1956; Van der Hoven, 1957; Byzova et al., 1967; Kolesnikova and Monin, 1965) it is reasonable to conclude that spectra obtained over land contain gaps at mesoscale. Figs. 7, 8, and 9 all extend through the gap showing the existence of it under widely different conditions; figs. 7 and 8 were obtained in winter time under average weather conditions. Fig. 9, which is a component spectrum (see later), was obtained under summer conditions with light winds and strong convection during daytime; also here a definite but narrow gap is displayed. The lifting in the high-frequency ends of the spectra is the combined effect of the spectra penetrating into the region near the microscale maximum and of aliasing. The fact that the spectra from Station Nord, fig. 10, and the spectra from all the heights of the Risø Tower, figs. 11, 12, 13, 14, 15, 16, and 17, all fall rapidly off in the mesoscale region, although they do not extend through the gap, is consistent with a gap. The estimated effects of aliasing on the

Risø Tower data can be seen on fig. 2.

In section 5.4 it will be shown to what extent a spectrum calculated from speed data resembles $S_{ii}(\omega)$ (from eq. 2.9), where the spectral analysis is performed on the component of the wind vector after two orthogonal horizontal axes and the resulting two spectra have been added (in the following $S_{ii}(\omega)$ will be called the component spectrum or the U+v spectrum). From figs. 21, 22, 23, and 24 we note that the component spectra calculated for the heights 7, 56, and 123 m at the Risø Tower and that from Station Nord all fall off in the mesoscale region even more rapidly than the speed spectra. This is fortunate because, as we shall see in section 5.4, the component spectrum gives a much better representation of energies on scales than does the speed spectrum.

Millard (1968) measured a composite spectrum over the sea which shows an extremely high amount of energy in the high-frequency end and a deep gap through the whole mesoscale region. However, because microscale turbulence is generally weak over the ocean, one would suspect the high frequency energy to originate from buoy motions.

Using the hypothesis that a spectral gap occurs in time spectra of the wind over land, it is possible to design experiments that will provide information of significance for the understanding of the behaviour of the atmosphere. Such experiments should be carried out giving simultaneous measurements of the synoptic scale fields, of the internal structure of ensembles of microturbulence, and of the bulk properties of microturbulence ensembles. Using these three sets of measurements, the internal structure of the microturbulence ensembles should be related to the synoptic scale environment, the bulk properties of the microturbulence ensembles should be explained in terms of their internal structure, and finally the bulk properties of the turbulence ensembles should be used to parameterize the effects of microturbulence on the synoptic scale fields in terms of synoptic scale variables.

The internal structure of atmospheric microturbulence in the lowest thirty metres of the planetary boundary layer has been explored in greatest detail over the last decades and it seems it can be predicted, to a fair degree of accuracy, when a not too complicated synoptic-scale field is specified (see e.g. N.E. Busch, 1973). Also other forms of microturbulence, as for example Clear-Air-Turbulence, have been studied with success (J.A. Dutton and H.A. Panofsky, 1970). Still, much more needs to be known about the physical structure of the regions of turbulence and their dependence upon the large scale variables, and even with very detailed knowledge at hand, a

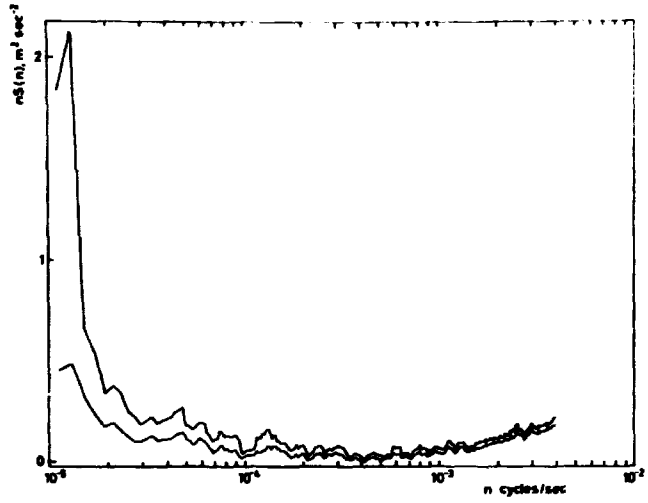

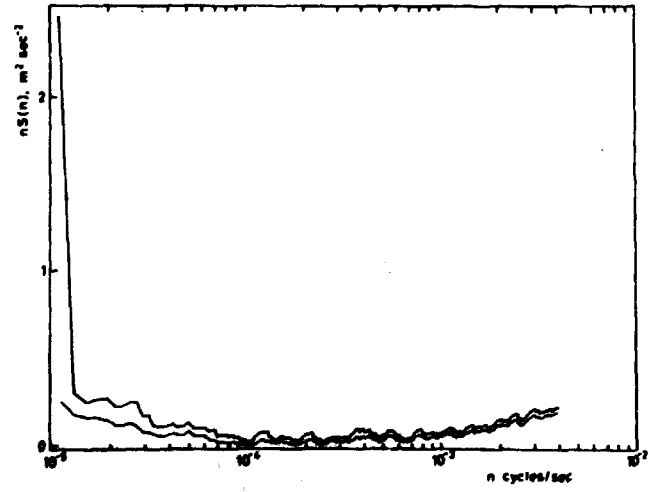

Fig. 7, top and fig. 8, bottom. Spectra of the horizontal wind speed at 8 m height based on two records, each of one week's duration, measured at Risø in the winter of 1971-1972. The plotted curves are the confidence limits, cf. section 6.4.

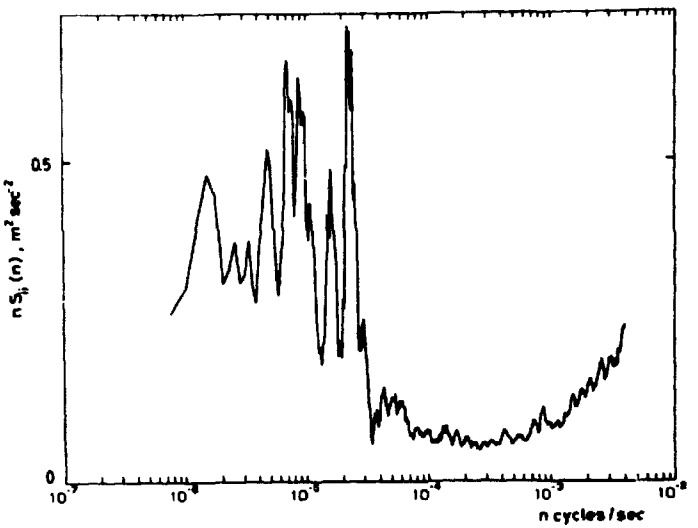

Fig. 9. Spectrum of the horizontal wind vector. Measured at a height of 12 m in the summer of 1972 at Karlstrup, Zealand.

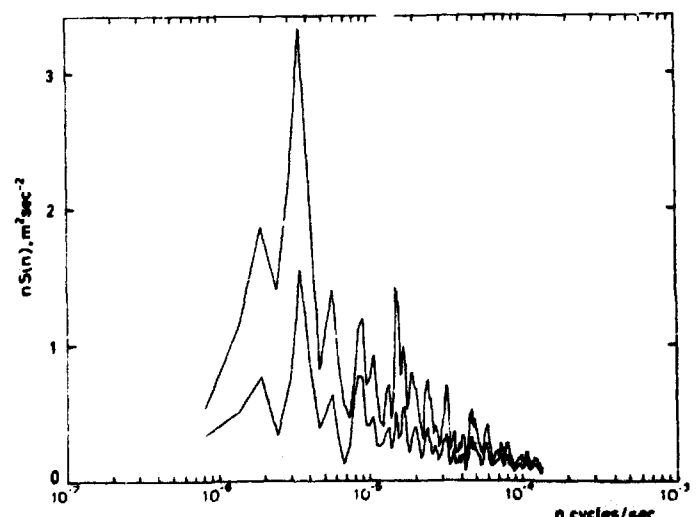

Fig. 10. Spectrum of the horizontal wind speed. Measured at a height of 5 m in the summer of 1972 at Station Nord, Greenland. The plotted curves are the confidence limits, cf. section 4.4.

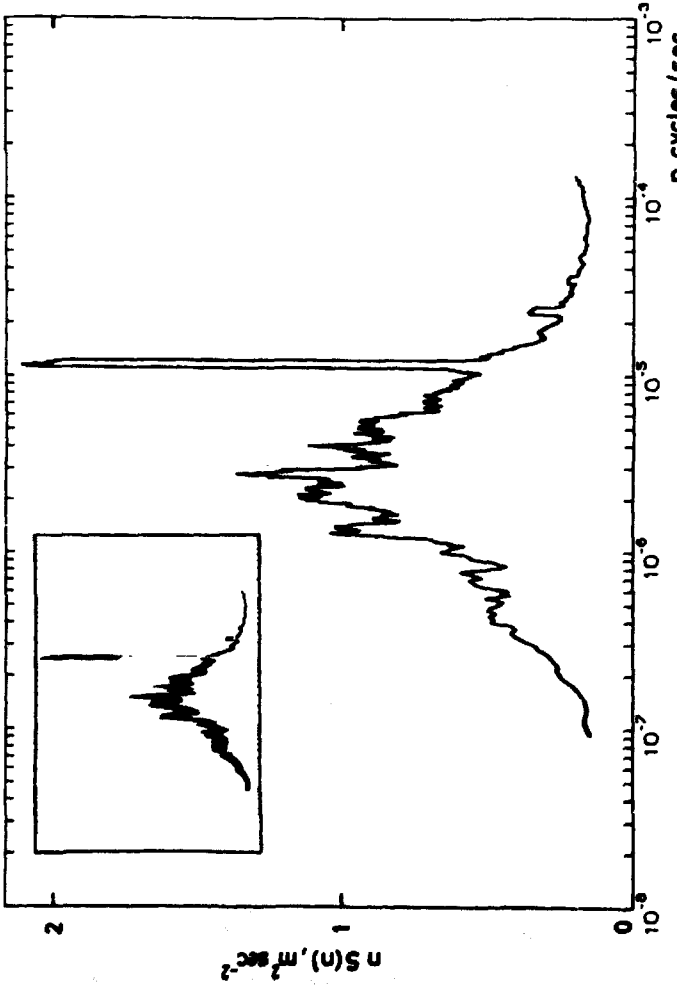

Fig. 11. Spectrum of the horizontal wind speed. Measured at a height of 7 m, Risø 1958-67. For this and the following six figures, confidence limits are as displayed on the inserted figure.

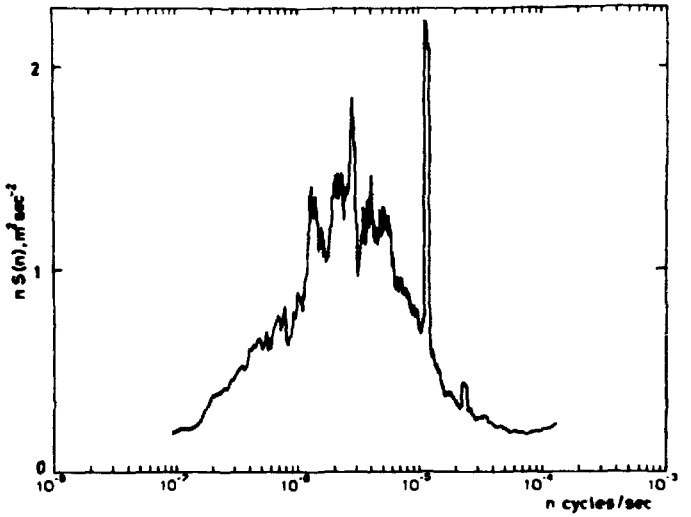

Fig. 12. Spectrum of the horizontal wind speed. Measured at a height of 23 m. Risø 1958-67.

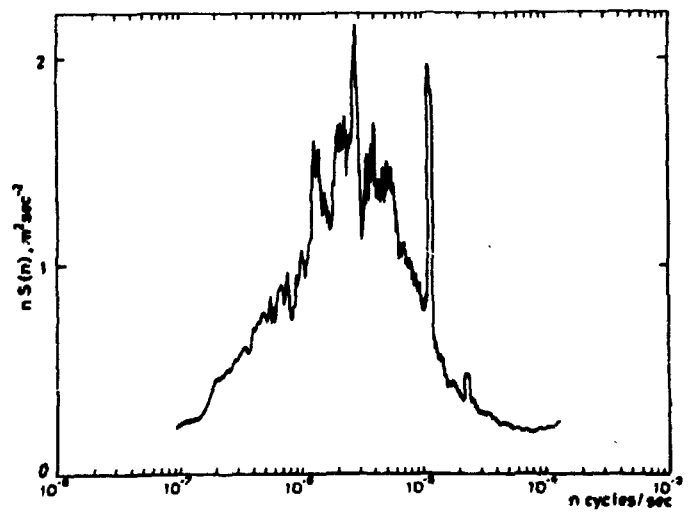

Fig. 13. Spectrum of the horizontal wind speed. Measured at a height of 39 m, Risø 1958-67.

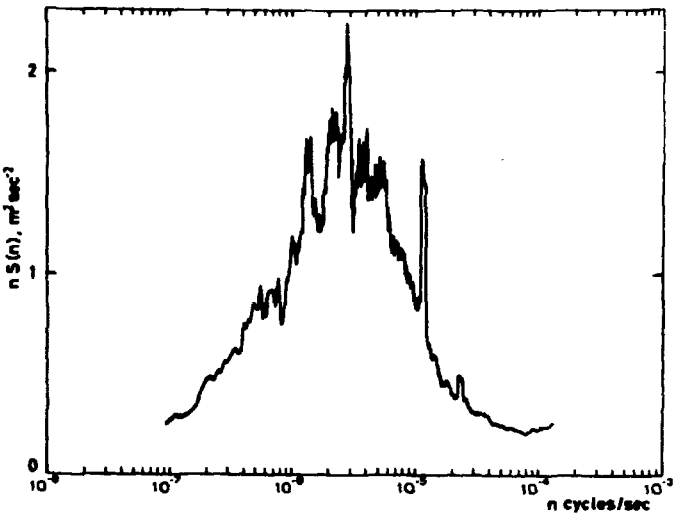

Fig. 14. Spectrum of the horizontal wind speed. Measured at a height of 56 m. Risø 1958-67.

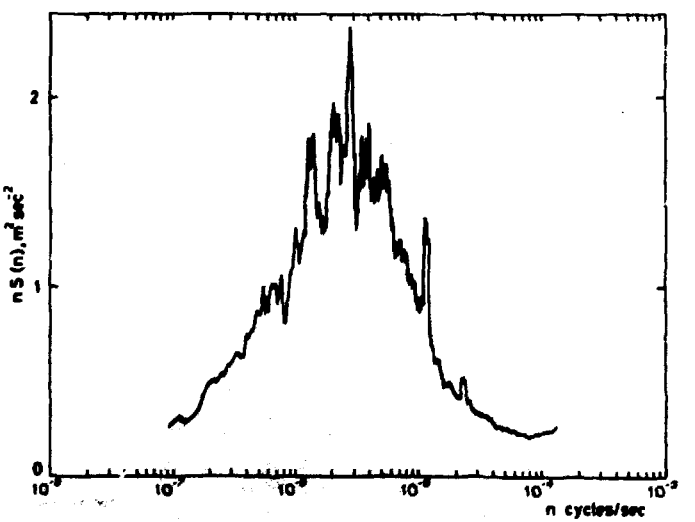

Fig. 15. Spectrum of the horizontal wind speed. Measured at a height of 72 m, Risø 1958-67.

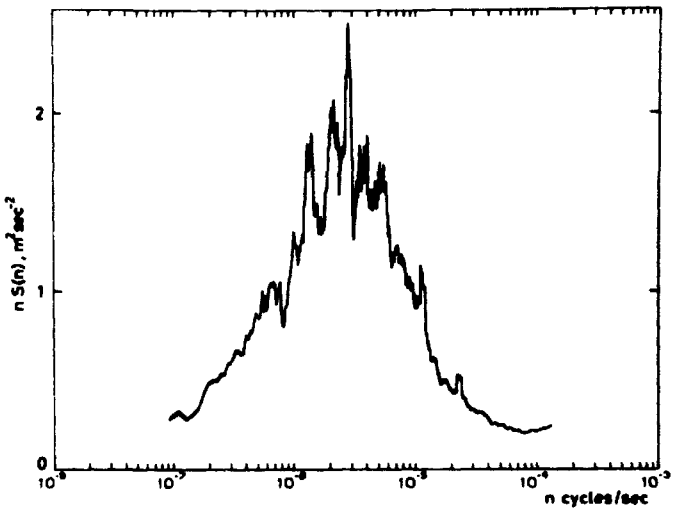

Fig. 16. Spectrum of the horizontal wind speed. Measured at a height of 96 m, Riso 1958-67.

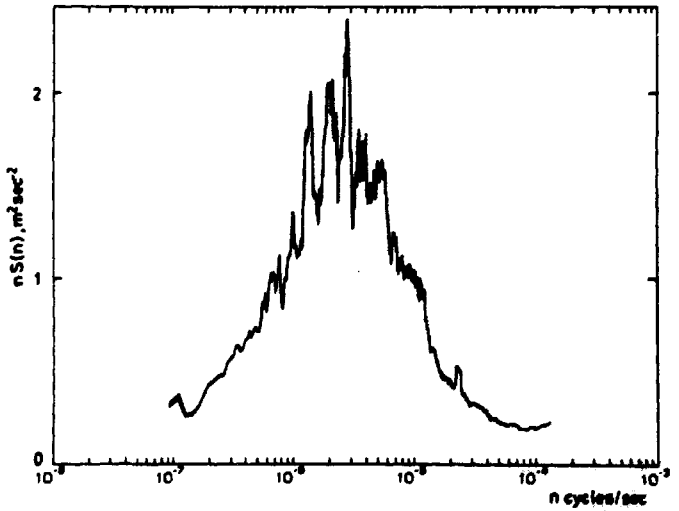

Fig. 17. Spectrum of the horizontal wind speed. Measured at a height of 123 m, Riso 1958-67.

crucial point in using this information in weather prediction models is the prodiction of the future distribution of turbulence activity on the basis of synoptic scale information.

5.2.2. An Explanation of the Spectral Gap

Seeking a physical understanding of the mechanisms in the atmosphere leading to a gap in the mesoscale region, we note that the atmosphere is relatively thin; its effective depth, approximately 10 km, is small compared to its horizontal extent, which is 40,000 km. Hence the main groups of scales could be classified as follows: the synoptic region with scales large compared to depth, the motions being almost two-dimensional; the micrometeorological region with scales less than the depth and with three-dimensional motions; the mesometeorological region with scales from a few km up to hundreds of km and with both two- and three-dimensional motions.

The equal shapes of the spectra on fig. 6 indicate that it should be easy to explain why the motions on the synoptic and micro scales are so energetic compared to the motions on mesoscales. On the other hand, the atmospheric motions are fueled on many different scales, such as large scale differential heating between pole and equator, differential heating between land and sea, latitudinal heating received on the rotating spherical earth, latent heat and potential energy associated with cyclones or local thunderstorms. Thus, the manner in which solar energy is converted into atmospheric motion is indeed very complicated, and no complete theory is available for the development of this motion on all scales. However for the present purpose it is sufficient to observe that kinetic energy is mainly fed on two different scales and by two different processes. The large-scale differential heating results in the birth of ultralong waves with wavelengths of the order of thousands of km. Through baroclinic processes, the energy thus made available is transformed into kinetic energy of the waves at the higher harmonics reaching into the region with baroclinically unstable waves which tend to grow at the expense of potential and internal energy.

At the other end of the spectrum an instability due to vertical wind shear produces kinetic energy. If the Richardson number ($Ri = (-g/\rho)(\partial\rho/\partial z)(\partial v/\partial z)^{-2}$) is somewhat less than 0.25, eddies with wavelengths of the order of km are produced. When the Richardson number becomes negative, hydrostatic instability is released, which produces eddies of the same size as those produced by wind shear. Thus, we find two main wavelength-domains, widely separated, where instabilities and kinetic energy are produced.

For the sake of completeness it should be mentioned that there are processes occurring in the atmosphere which produce kinetic energy in the mesoscale range such as gravity waves, land-sea-breeze systems and diurnal variations. We may suspect that these systems narrow the gap and fill it up under certain conditions. Fig. 9 displays how under light wind and frequent convection conditions the spectral gap can be narrowed, especially from the low frequency end; probably some land-sea-breeze systems occurred during the 42 days of measurements.

There are two customary approaches for the mathematical treatment of the development of fluid motions on various scales: either to consider the stability properties of disturbances in the flow or to extend the Reynolds formulation of the turbulence problem into the domain of scale, using Fourier analysis.

Stability studies can indicate wavelength regions into which energy is fed, but the method has at least one serious drawback: no information is given as to the transfer and transformation of energies among various scales of eddy motion. Because of these interactions, it is not possible to determine the shape of the spectrum from a specification of the energy input to the spectrum; in fact the exchange mechanisms may occasionally tend to concentrate the spectral energy in certain bainds.

The interaction between scales is usually studied using spectral equations of the atmospheric motions, either in wave number space (B. Saltzman, 1957; J. A. Dutton, 1963; Kao, 1968) or in frequency space (Kao, 1968; W.C. Chiu, 1970). In the next chapter we shall derive the spectral equations in frequency space to see if important implications can be revealed by these equations concerning the shape of the spectrum.

5.3. The True Periodicities in the Spectrum

The most significant discrepancy between the three spectra on fig. 6 is found at the frequency $1.16 \cdot 10^{-5}$ Hz, which is easily identified as the diurnal cycle of the wind velocity. The Risø spectra display a very prominent peak at this frequency. Fiedler's spectrum has a noticeable peak but in Van der Hoven's spectrum the dirnal peak is non-existent.

A.H. Oort and A. Taylor (1969) made a very comprehensive analysis of the diurnal peaks in spectra calculated for six stations in the north-eastern parts of the United States using 10 years' hourly, one-minute average, observations of surface wind speed. All their spectra substantiated the features of the Risø spectrum with very large peaks at the dirunal frequency. Oort and Taylor explained the difference between their own and Van der Hoven's

results concerning the diurnal cycle from the difference in heights, approximately 10 and 100 m, in which the measurements were taken, (in fact also Van der Hoven attributed the lack of a one-day spectral peak in his spectrum to the height of observation). The series of figs. 11 to 17 depicts this explanation very nicely. However, from the former chapters we know that true periodicities should be removed from the records before performing the spectral analysis; the reason for not doing this is that no feasible method exists (although the method worked out by N.E. Busch and E.L. Petersen (1970), mentioned in chapter 4, has shown to be promising; however, it requires an enormous amount of labour). We have adopted the attitude not to subtract any suspected periodicity from the series but rather keep check on its possible influence on the spectrum. The smoothing procedure and the plotting convention used are tuned to treat a continuous spectrum and no special treatment is given to spectral lines. This means for example that the spectral peak in fig. 11 is averaged over a number of estimates determined by the filter width used in the smoothing. Becuase only one or two estimates give the spectral line, the width of the diurnal peak as given by the spectrum is about equal to the constant relative bandwidth used in the smoothing.

To give a more representative picture of the daily and yearly variations of the wind speed as revealed by the spectral analysis we selected the raw amplitudes before smoothing and plotted them in fig. 18. Taking the yearly variations first, we plotted the mean wind speed calculated for every month in fig. 19, and found good agreement between the two figures, both, however, giving evidence of common knowledge. The curve in fig. 18 exhibits the variation of the diurnal oscillation with height and shows a tendency towards a minimum between 96 and 123 m, which indicates a further growth in the amplitude with height. This is in agreement with an investigation by Byzova et al. (1968), where a daily cycle was found up to a height of 300 m. Even the spectrum given by N.K. Vinnichenko (1970) for heights of 3 to 20 km shows a daily peak.

However, fig. 18 gives only a very rough picture of how the diurnal variation takes place in the lowest 120 m of the atmosphere. We shall return to the question in chapter 7, but let us note from the figures in that chapter (fig. 31): the level with minimum daily variation varies throughout the year from 50 m in December to several hundred m in the summer. When we consider a single height not only the amplitude is subject to variation from month to month, but also the form along the time axis is, figuratively, stretched in the summer and compressed in the winter. To investigate how

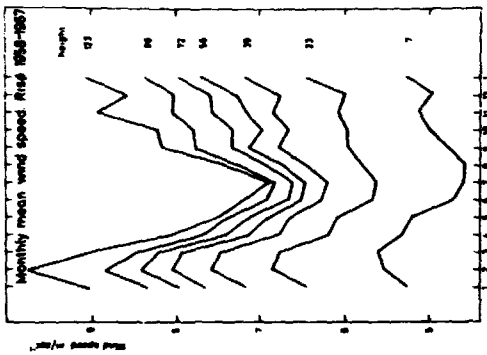

Fig. 16. The variation of the monthly mean wind speed through the year shown for seven heights.

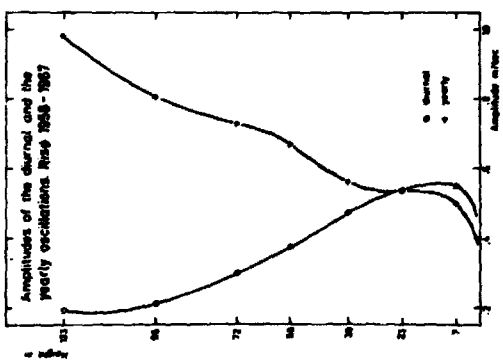

Fig. 18. Amplitudes of the diurnal and yearly variations as estimated from Fourier decompositions of the measured wind speeds from the indicated heights.

this may affect the spectrum, the hourly average wind speed curves for every month, as given by fig. 31, were expanded into Fourier series. The result of this analysis is depicted in table 3, where the percentage of the variance explained by the first and the second harmonics, (i.e. with periods of 24 and 12 hrs) is given. It is obvious that a deformation of the daily cycle mainly results in an increase of the amount of variance explained by the second harmonic. This is revealed by figs. 12 to 17 showing how the magnitude of the variance caused by the daily variation becomes comparable to the variance in the adjacent frequency intervals. The figures also show that the distortion of the daily cycle causes an amount of variance to be given by the second harmonic, which is large compared to the variance of the surrounding frequencies. From the figures we see that whereas we cannot distinguish the daily peak at a height of 123 m, we can easily distinguish the 12-hour peak at all heights.

Many speculative arguments have been propounded in the literature to explain the semidiurnal peak as being caused by one single physical effect; for instance atmospheric tides and inertial oscillations. We feel that it is the daily cycle in the planetary flow field (over land), set up by the daily cycle in the insolation, that causes the occurrence at spectral lines at the diurnal period and the corresponding higher harmonics. The distribution of the energies on the different frequencies depends on how the flow field reacts to the cycle in the solar radiation. Many effects have to be taken into account, such as pressure forces, Coriolis forces, and the distribution of microturbulence. Introducing the periodicity in the radiation into the set of equations governing atmospheric motions also means (in the simplified cases where the equations can be solved) the introduction of a similar periodicity into the flow field, but not a clean periodicity of half the period.

In the next section we shall see quite a different effect that may add to the size of the second harmonic in speed spectra in the case where the diurnal cycle in the speed is accompanied by a large daily turning of the wind vector.

Month \ Height m	7	23	39	56	72	96	123
1	24	31	44	72	77	79	82
	50	38	26	13	11	8	9
2	70	74	77	71	65	56	62
	22	15	9*	4*	1*	18	27
3	88	88	88	86	84	83	31
	11	10	10	11	11	7	14*
4	92	92	90	85	82	70	78
	5	7	9	13	16	20	18
5	94	93	90	84	76	52	37
	3	4	7	13	20	41	51
6	95	94	92	88	80	65	43
	3	4	6	11	18	30	49
7	95	94	92	89	83	65	33
	3	4	6	10	16	32	53
8	93	91	90	88	86	72	58
	5	7	8	10	12	20	28
9	90	88	87	85	82	78	76
	9	10	11	13	14	10	3*
10	82	81	80	80	76	78	74
	13	14	13	9*	7*	3*	14
11	81	84	87	80	22	24	34
	11	8	3*	18	56	65	58
12	72	55	52	20	28	49	42
	1*	3*	9	49	55	40	47

Table 3. Results of a Fourier decomposition of the 84 wind speed curves in fig. 31. For each of the twelve months in the year, these curves reveal the average daily variation, both in time and with height, of the wind speed as measured at the Risø Tower during the ten years 1958-67. The numbers in the table are, for each height and month, the percentages of variance explained by the first and second harmonics, i.e. one and two cycles per day, respectively. An asterisk indicates that the third harmonic is greater than the second harmonic.

5.4. Speed Spectra versus Component Spectra

Up to this point we have mainly presented speed spectra, i.e. spectra of the magnitude of the horizontal wind vector.

In an analysis earlier mentioned, Oort and Taylor (1969) presented the separate energy spectra of the south-to-north (v) and the west-to-east (u) components of the horizontal wind vector. A comparison between the speed spectra and the added u+v spectra revealed two interesting features for which they were unable to find adequate explanations. First, there was a significant increase of almost a factor of three in the total variance going from speed spectra to u+v spectra. Second, important diurnal cycles in the zonal and in the meridional wind components were lacking.

Several conventional meteorological wind sensing devices measure the wind in terms of horizontal speed and direction. Some, such as cup anemometers, measure speed only. Thus an analysis of the wind in terms of speed alone is not only convenient, but is sometimes all that is possible; therefore it is important to know the effects causing the differences between speed spectra and component spectra.

From the Reynolds convention $u_i = \langle u_i \rangle + u_i'$, where $u_1 = u$, $u_2 = v$.
Let $V = \sqrt{u^2 + v^2}$

$$\langle u_i\, u_i \rangle = \langle (u_i' + \langle u_i \rangle)\,(u_i' + \langle u_i \rangle) \rangle = \langle u_i'^2 \rangle + \langle u_i \rangle^2,$$

i.e. total kinetic energy = mean kinetic energy + eddy kinetic energy

$$= \langle u_i \rangle^2 + \langle u_i'^2 \rangle = \mu_i^2 + \sigma_i^2 =$$

$$= \langle u_i \rangle^2 + \int_{-\infty}^{\infty} S_{ii}(\omega)\, d\omega .$$

For the speed we have $\langle \sqrt{u^2 + v^2}\ \sqrt{u^2 + v^2} \rangle = \langle u^2 \rangle + \langle v^2 \rangle$, so the total kinetic energy is the same whether we use component measurements or speed measurements.

To understand how the differences between speed spectra and component spectra originate, let us first consider an example with small fluctuations in the wind field.

We have

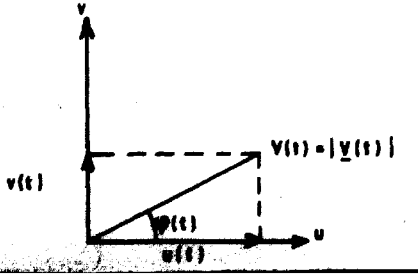

Using Taylor expansion, we can write for a function $f(x)$

$$\langle f(x) \rangle = \langle f\left(\langle x \rangle + (x - \langle x \rangle)\right) \rangle \approx$$

$$\langle f(\langle x \rangle) \rangle + \langle f'_x(\langle x \rangle)(x - \langle x \rangle) \rangle + \frac{1}{2} f''_x(\langle x \rangle)(x - \langle x \rangle)^2 \rangle =$$

$$f(\langle x \rangle) + \frac{1}{2} f''_x(\langle x \rangle) \sigma_x^2$$

(here $f'_x(x)$ denotes the derivatives of $f(x)$ with respect to x).

And for a function of two variables $f(x,y)$

$$\langle f(x,y) \rangle \approx f(\langle x \rangle, \langle y \rangle) + \frac{1}{2} f''_x(\langle x \rangle, \langle y \rangle) \sigma_x^2$$

$$+ f''_{xy}(\langle x \rangle, \langle y \rangle) \rho_{xy} \sigma_x \sigma_y + \frac{1}{2} f''_y(\langle x \rangle, \langle y \rangle) \sigma_y^2, \qquad (5.2$$

where $\rho_{xy} \sigma_x \sigma_y = \langle (x - \langle x \rangle)(y - \langle y \rangle) \rangle$.

Using Eq. (5.2) : (and u_1 and u_2 instead of u and v)

$$\langle u_1 \rangle = \langle V\cos\varphi \rangle = \langle V \rangle \cos\langle \varphi \rangle - \frac{1}{2} \langle V \rangle \cos\langle \varphi \rangle \sigma_\varphi^2 - \sin\langle \varphi \rangle \rho_{v_\varphi} \sigma_v \sigma_\varphi$$

$$\langle u_2 \rangle = \langle V\sin\varphi \rangle = \langle V \rangle \sin\langle \varphi \rangle - \frac{1}{2} \langle V \rangle \sin\langle \varphi \rangle \sigma_\varphi^2 + \cos\langle \varphi \rangle \rho_{v_\varphi} \sigma_v \sigma_\varphi .$$

Without losing generality the coordinate system can be chosen so that $\langle \varphi \rangle = 0$

$$\langle u_1 \rangle = \langle V \rangle \left(1 - \frac{\sigma_\varphi^2}{2}\right),$$

$$\langle u_2 \rangle = \rho_{v_\varphi} \sigma_v \sigma_\varphi ,$$

$$\sigma_{u_1}^2 = \langle u_1 - \langle u_1 \rangle \rangle^2 = \langle u_1^2 \rangle - \langle u_1 \rangle^2 = \langle V^2 \cos^2\varphi \rangle - \langle u_1 \rangle^2 =$$

$$\langle V \rangle^2 + \sigma_V^2 - \langle V \rangle^2 \sigma_\varphi^2 - \langle V \rangle^2 (1 - \sigma_\varphi^2 + \frac{1}{4} \sigma_\varphi^4)$$

$$\approx \sigma_V^2 ,$$

$$\sigma_{u_2}^2 = \langle u_2 - \langle u_2 \rangle \rangle^2 = \langle u_2^2 \rangle - \langle u_2 \rangle^2 = \langle V^2 \sin^2\varphi \rangle - \langle u_2 \rangle^2$$

$$= \langle V \rangle^2 \sigma_\varphi^2 - \rho_{v_\varphi}^2 \sigma_v^2 \sigma_\varphi^2 = \langle V \rangle^2 \sigma_\varphi^2 \left(1 - \rho_{v_\varphi}^2 \frac{\sigma_u^2}{\langle V \rangle^2}\right)$$

$$\approx \langle V \rangle^2 \sigma_\varphi^2 .$$

In the approximations we have used the assumption of small fluctuations (compared to $\langle V \rangle$) and $\rho_{v_\varphi} \ll 1$.

We have: $\sigma_{u_1}^2 + \sigma_{u_2}^2 \cong \sigma_V^2 + \langle V \rangle^2 \sigma_\varphi^2$, which shows that the difference between the areas of the component spectrum and the speed spectrum is of the order $\langle V \rangle^2 \sigma_\varphi^2$ (for the case considered). For a fixed $\langle V \rangle$, the difference is determined by the fluctuations in the wind direction.

To shed some more light on the differences between the two types of analysis, we will use a simple numerical model with large fluctuations in the wind field and thereby show that if fluctuations on certain frequencies result in high spectral values in the component spectrum, and at the same time cause significant variations in the wind direction, then most of their contribution will be lost in the speed spectrum.

The model is:

$$u_1(t) = A_1 \cos(\omega t) + A_2 \cos(8\omega t) + B$$

$$u_2(t) = 0 ,$$

i. e. two wind fields are superposed upon a steady flow from west to east, each field oscillating in this direction but with different periods.

Let $A_1 = A_2 = 1$

$$\omega = 2\pi/T .$$

The flow field is sampled at 64 equidistant time intervals through the time $0 \le t \le T$, and the experiment is carried out 16 times with B varying from 0 to 1.5 in steps of 0.1.

Regardless of the value of B, a component analysis will always result in a spectrum consisting of two lines, one at the first harmonic and the other at the eighth harmonic, each accounting for 50 % of the variance. ($\sigma_{u_1} = 1$ and $\sigma_{u_1} = B$).

The speed measured by a cup anemometer will be:

$$V(t) = | u_1(t) | = | A_1 \cos(\omega t) + A_2 \cos(8\omega t) + B | .$$

If $B = A_1 \cos(\omega t) + A_2 \cos(8\omega t)$ for all t there will be no difference between the speed spectrum and the component spectrum. If B does not fulfil this condition the effect can be rather drastic as shown in fig. 20 with eight speed spectra. The values of B, μ_v, and σ_v^2 are given on every figure; only 17 of the possible 32 harmonics are shown because no noticeable variance is given by the harmonics higher than the 16th.

We see quite a different division of kinetic energy into mean kinetic energy (μ^2) and eddy kinetic energy (σ^2). In the example where B = 0 there is no energy in the mean flow and the eddy energy = 1, whereas in the analysis of speed data 64% of the energy appears as energy of the mean flow. Further in the speed spectrum practically no energy is found at the first harmonic, but some of it can be found on the second harmonic; the energy of the eight harmonic is spread to adjacent harmonics and to the 16th harmonic. The changes caused by the growth of B are clearly revealed by the picture, hence let us apply ourselves to the measurements again.

In figs. 21, 22, and 23 for each of the heights 7, 56, and 123 m at the Risø Tower the four spectra are plotted on the same figure: speed, u, v, and u + v. A small scheme inserted in the figures indicates how the total kinetic energy, K_t, is distributed between mean kinetic energy, K_m, and eddy kinetic energy, K_e. The overall loss in eddy energy going from u+ v to speed spectra is 73% of the total energy at 7 m, 77% at 56 m, and 83% at 123 m.

The lack of correspondence between K_t as calculated for the u+ v and for the speed spectra is due to the different ways of estimating missing observations for the two spectral calculations.

All the frequency bands in the speed spectra have energies less than those of the corresponding component spectra, but the regions worst affected are those on the synoptic scale that are associated with migratory cyclones and anticyclones, i.e. systems with large fluctuations in the wind direction.

In his re-analyses of Oort and Taylor's data, L. L. Wendell (1970) found the same features in the spectra and he further pointed out that rather than lack of an important diurnal cycle in the zonal and meridional wind components, as found by Oort and Taylor, the contribution to the variance by the synoptic scale disturbances is far more significant than revealed by the speed spectrum. This is clearly shown by figs. 21, 22, and 23.

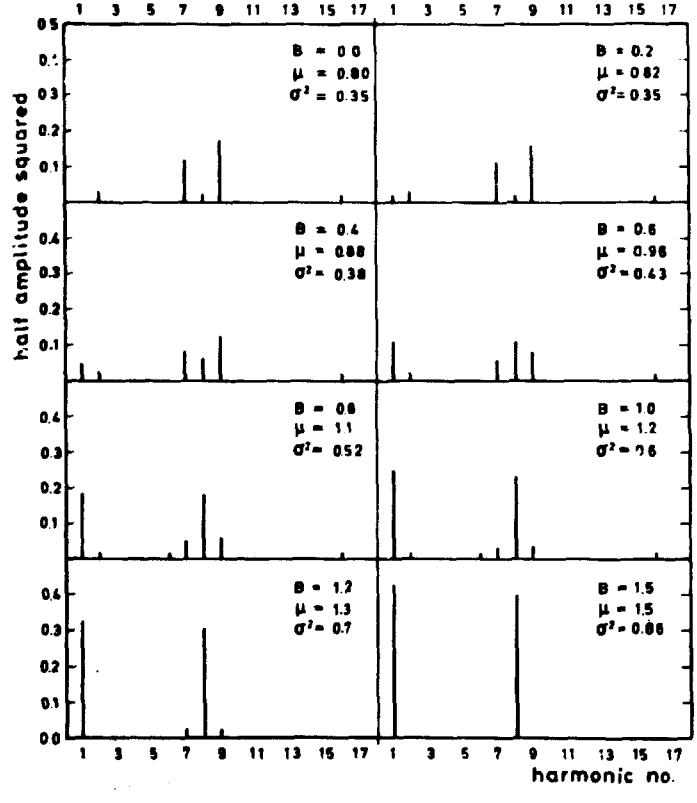

Fig. 20. The result of a digital Fourier decomposition of the function $u_1(t) = | \cos(\omega t) + \cos(8\omega t) + B |$ with B varying as given on the figure. μ is the mean value and σ^2 the variance.

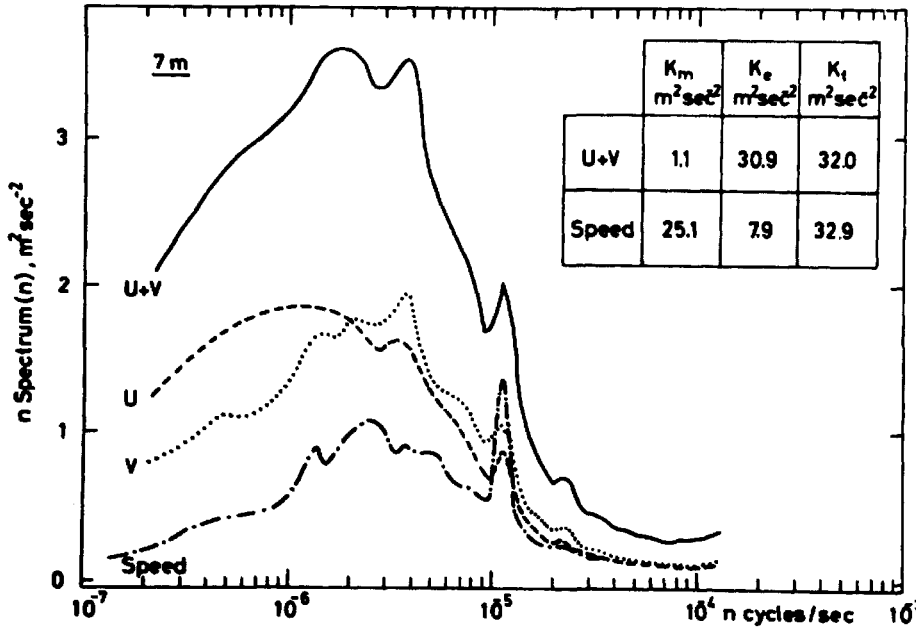

Fig. 21. Comparison of wind speed and component spectra. Measured at Rise 1958-67 at a height og 7 m.

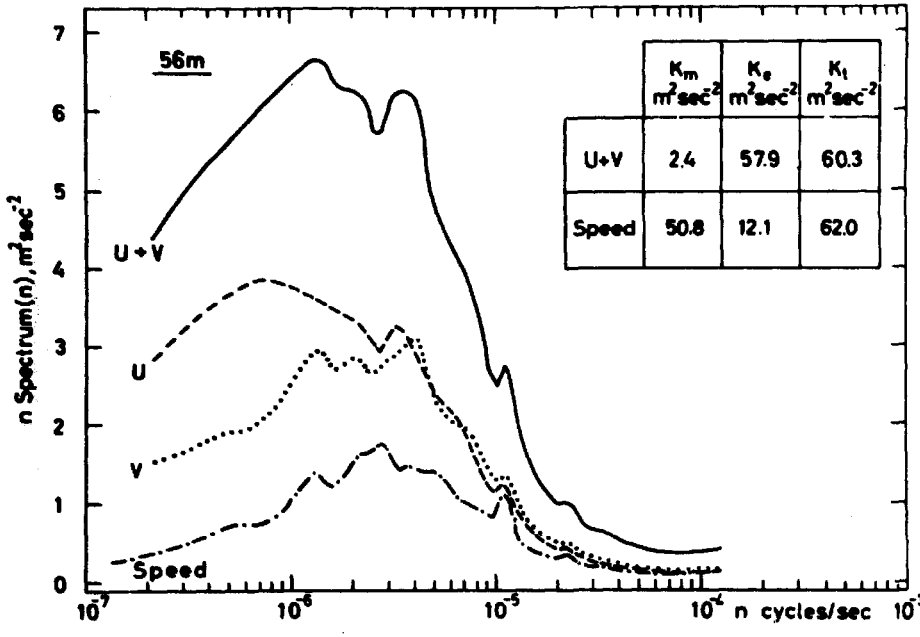

Fig. 22. Comparison of wind speed and component spectra. Measured at Rise 1958-67 at a height of 56 m.

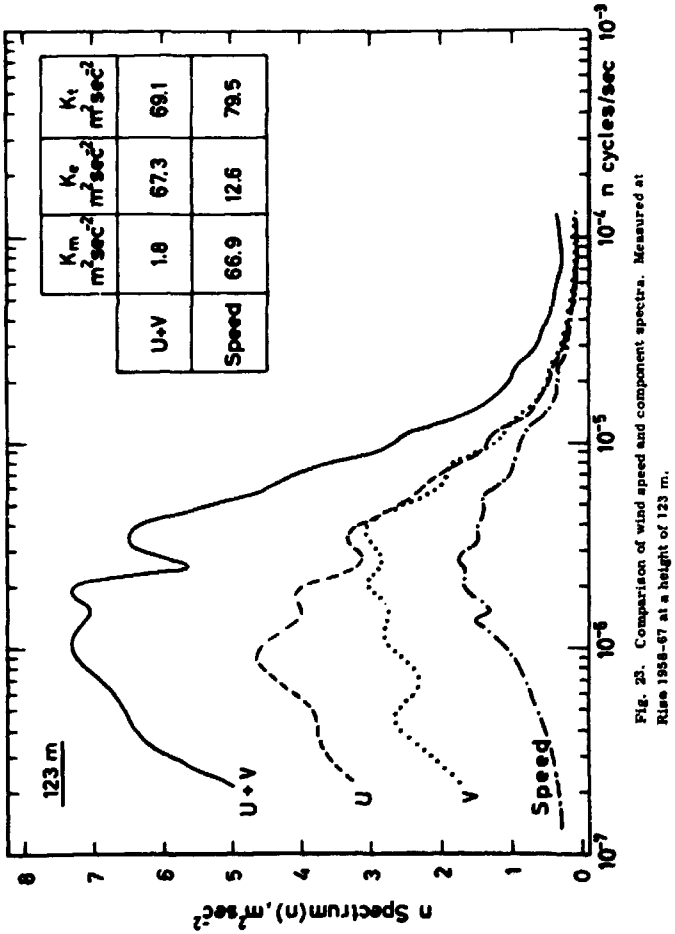

Fig. 23. Comparison of wind speed and component spectra. Measured at Risø 1958-67 at a height of 123 m.

The conclusion of this section is that an analysis of speed data alone does not realistically represent the diversion of the total energy into eddy energy and energy of the mean flow; neither does the analysis give any realistic distribution of the eddy energy over the appropriate range of frequencies.

5.5. The Effects on the Component Spectra Caused by a Rotation of the Coordinate System

In his analysis, Wendell further investigated the effect of a rotation of the component axes. Recomputing the spectra for many orientations of the axes he found that with a 49° clockwise rotation practically all the eddy energy was in the v component. His measurements for this analysis were obtained at the National Reactor Testing Station, Idaho, located on the Upper Snake River Plain. This plain is approximately 69 miles wide and bounded on both sides by mountains oriented NE-SW. He concluded that the mountain barriers tend to channel the flow over the plain in a north-easterly south-westerly orientation, and this indicates that a component analysis performed as a rotation-of-the-axis-analysis might reveal significant surface effects on the flow.

The Risø Tower data were subjected to a "rotation-analysis" but instead of calculating the Fourier transforms for small intervals of degrees around the compass card, we did the following:

The u-v coordinate system, where we performed the one-component analysis, is rotated clockwise through the angle θ:

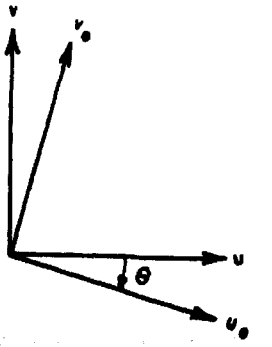

and here u, v, u_θ, and v_θ denote deviations from the mean values.

$$u_\theta = u \cos\theta - v \sin\theta ,$$

$$v_\theta = v \cos\theta + u \sin\theta ,$$

$$\langle u_\theta v_\theta \rangle = \langle (u\cos\theta - v\sin\theta)(v\cos\theta + u\sin\theta) \rangle$$

$$= \langle uv \rangle (\cos^2\theta - \sin^2\theta) + (\langle u^2 \rangle - \langle v^2 \rangle)(\cos\theta \sin\theta)$$

$$= \langle uv \rangle \cos 2\theta + \frac{1}{2}(\langle u^2 \rangle - \langle v^2 \rangle) \sin 2\theta ,$$

$$\langle u_\theta^2 \rangle = \langle (u\cos\theta - v\sin\theta)(u\cos\theta - v\sin\theta) \rangle$$

$$= \langle u^2 \rangle \cos^2\theta + \langle v^2 \rangle \sin^2\theta - \langle uv \rangle \sin 2\theta ,$$

$$\langle v_\theta^2 \rangle = \langle (v\cos\theta + u\sin\theta)(v\cos\theta + u\sin\theta) \rangle$$

$$= \langle v^2 \rangle \cos^2\theta + \langle u^2 \rangle \sin^2\theta + \langle uv \rangle \sin 2\theta ,$$

$$\frac{\partial \langle u_\theta^2 \rangle}{\partial \theta} = (\langle v^2 \rangle - \langle u^2 \rangle) \sin 2\theta - 2\langle uv \rangle \cos 2\theta ,$$

$$\frac{\partial \langle v_\theta^2 \rangle}{\partial \theta} = -(\langle v^2 \rangle - \langle u^2 \rangle) \sin 2\theta + 2\langle uv \rangle \cos 2\theta ,$$

We assume $\langle v^2 \rangle \neq \langle u^2 \rangle$ and $\langle uv \rangle \neq 0$ and then have:

$$\langle u_\theta v_\theta \rangle = \frac{\partial \langle u_\theta^2 \rangle}{\partial \theta} = \frac{\partial \langle v_\theta^2 \rangle}{\partial \theta} = 0 \text{ for } \tan 2\theta = \frac{2\langle uv \rangle}{\langle v^2 \rangle - \langle u^2 \rangle} .$$

A discussion of signs shows that $\langle v_\theta^2 \rangle$ is maximum, $\langle u_\theta^2 \rangle$ minimum and $\langle u_\theta v_\theta \rangle = 0$ for the following combinations:

$$\langle uv \rangle > 0 \begin{cases} \langle v^2 \rangle > \langle u^2 \rangle & : \quad -0 < \theta < \frac{\pi}{4} \\ \langle v^2 \rangle < \langle u^2 \rangle & : \quad -\frac{\pi}{4} < \theta < \frac{\pi}{2} \end{cases}$$

$$\langle uv \rangle < 0 \begin{cases} \langle v^2 \rangle > \langle u^2 \rangle & : \quad -\frac{\pi}{4} < \theta < 0 \\ \langle v^2 \rangle < \langle u^2 \rangle & : \quad -\frac{\pi}{2} < \theta < -\frac{\pi}{4} . \end{cases}$$

Table 4 gives the calculated values for θ, $\langle u_\theta^2 \rangle$, and $\langle v_\theta^2 \rangle$ for three heights, and the result of the analysis is shown in the three figures. The

magnitudes of the wind vectors, 1.0 m/sec, 1.6 m/sec and 1.3 m/sec, are very small compared to the total fluctuating energies, 31 m^2/sec^2, 57 m^2/sec^2, and 67 m^2/sec^2, so we do not assign too much significance to their directions. For the top level the direction of maximum eddy energy is west-east, which we explain to be connected with the west-to-east movement of the cyclones, but we note that the distribution on maximum and minimum axes is 60% and 40%, respectively, of the total eddy energy. Thus in contrast to Wendell's analyses, there is no totally lopsided division of energy on components as a result of a rotation of the coordinate system. The same arguments can be used for the two lower levels, and we conclude that there are no channel effects. The fact that the u and v spectra nearly coincide from periods of time of the order of 4 days down to small periods makes us suspect that the flow exhibits some properties of isotropy in this range.

Height m	Mean East-West comp. m/sec.	Mean North-South comp. m/sec.	$\overline{u^2}$ m²/sec²	$\overline{v^2}$ m²/sec²	$\overline{uv}$ m²/sec²	$\frac{\tan 2\theta = \frac{2\overline{uv}}{\overline{v^2}-\overline{u^2}}}{}$	θ degrees	$\overline{u^2_\theta}$ m²/sec²	$\overline{v^2_\theta}$ m²/sec²
7	0.64	0.81	16.56	14.38	- 1.95	1.46	- 62	13.23	17.70
56	1.21	0.97	33.45	24.44	- 5.23	0.85	- 70	22.12	35.77
123	0.48	1.25	40.50	28.86	- 0.80	0.03	- 90	28.86	40.50

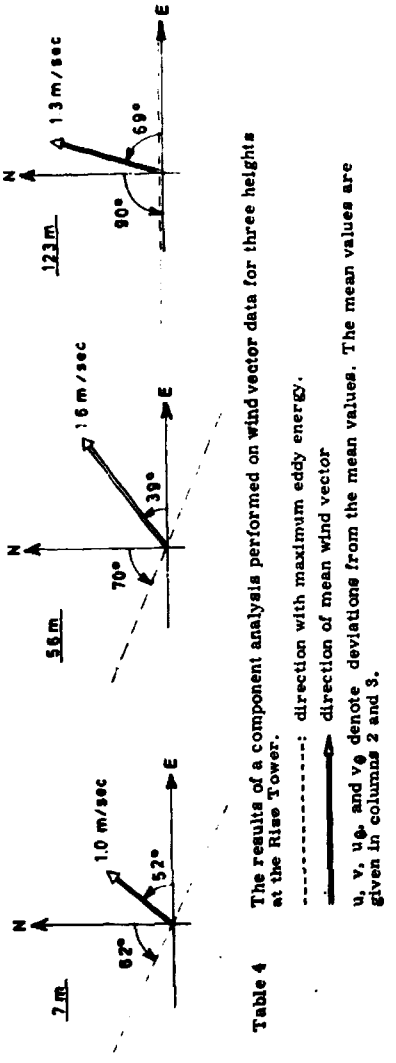

Table 4 The results of a component analysis performed on wind vector data for three heights at the Rise Tower.

----------: direction with maximum eddy energy.

——————→ direction of mean wind vector

u, v, u_θ and v_θ denote deviations from the mean values. The mean values are given in columns 2 and 3.

6. SPECTRAL EQUATION IN FREQUENCY DOMAIN

6.1. The Governing Equation

The four basic variables describing a dry atmosphere without changes in composition are pressure p, temperature T, density ρ, and the three-dimensional wind vector $\underline{u}$. Four equations relate these variables to each other: the Navier-Stokes equation for a rotating fluid, a continuity equation, the equation of state and the first law of thermodynamics. The same equations apply to all scales from microturbulence to motions on global scales. If we want to consider all scales simultaneously the full set of equations must be used, but if we concentrate on small scale motions, effects such as the rotations of the earth can be neglected; on large scales we can neglect vertical accelerations, on mesoscales we are back to the full set of equations again because here no important simplifications are possible.

We shall not make a sophisticated analysis of the governing equations and their analogues in Fourier-space (see e.g. J.A. Dutton, 1963). Keeping in mind what kind of observations we are analysing, we shall only use the Navier-Stokes equation for a horizontal wind vector u_i, (i = 1, 2)

$$u_{i,t} + u_j u_{l,j} = -\frac{1}{\rho} p,i - f\varepsilon_{i3k}u_k + F_i \qquad (6.1)$$

in which i = 1, 2; j = 1, 2, 3; k = 1, 2, 3; and F_i is accelerations due to viscous forces. In these equations we ignore the terms resulting from the curvature of the earth and make the usual meteorological approximation in the Coriolis force. The coordinate system is tangent to the surface of the earth at some latitude φ.

The quantities in the equations (6.1) are all instantaneous values and, as described in chapter 2, we consider each of them as consisting of a climatological mean, a periodic component, and a deviation from these. That is

$$u_i = u_i(x,y,z,t) = u_i^c(x,y,z) + u_i^p(x,y,z,t) + u_i'(x,y,z,t) \qquad (6.2)$$

$$\rho = \rho(x,y,z,t) = \rho^c(x,y,z) + \rho^p(x,y,z,t) + \rho'(x,y,z,t)$$

$$p = p(x,y,z,t) = p^c(x,y,z) + p^p(x,y,z,t) + p'(x,y,z,t)$$

$$F_i = F_i(x,y,z,t) = F_i^c(x,y,z) + F_i^p(x,y,z,t) + F_i'(x,y,z,t)$$

Henceforward we do not write out the arguments x, y, and z.

6.2. The Spectral Equations

Let us multiply Eq(6.1) at the time t by the velocity deviation at the time t':

$$u'(t')_i\, u(t)_{i,t} + u'(t')_i\, u(t)_j\, u(t)_{i,j} =$$

$$- u'(t')_i \frac{1}{\rho(t)} P(t)_{,i} - f\varepsilon_{i3k}\, u(t')_i\, u(t)_k + u'(t')_i\, F_i(t). \qquad (6.3)$$

Because we have chosen t' and t as two independent variations we can write:

$$M(t,t') = u'(t')_i\, u(t)_{i,t} = \left[u'(t')_i\, u(t)_i \right]_{,t}.$$

Using the following transformations:

$$\eta = \eta(t',t) = t' ,$$

$$\tau = \tau(t',t) = t - t' ,$$

$$t = t(\eta,\tau) = \eta + \tau ,$$

$$t' = t'(\eta,\tau) = \eta ,$$

we have

$$M(t,t') = M\Big(t'(\eta,\tau),\, t(\eta,\tau)\Big) = N(\eta,\tau) = N\Big(\eta(t',t),\ \tau(t',t)\Big)$$

and

$$\left.\frac{\partial M(t,t')}{\partial t}\right|_{t' = \text{constant}} = \frac{\partial N}{\partial \eta}\frac{\partial \eta}{\partial t} + \frac{\partial N}{\partial \tau}\frac{\partial \tau}{\partial t} = \left.\frac{\partial N}{\partial \tau}\right|_{\eta = \text{constant}}$$

i.e.

$$\left[u'(t')_i\, u(t)_i \right]_{,t} = \left[u_i(\eta)_i\, u(\eta+\tau)_i \right]_{,\tau} = \left[u_i(t')_i\, u(t+\tau)_i \right]_{,\tau}.$$

Let u_i' be $u'(t')_i$, u_i be $u(t'+\tau)_i$, and P_i be $\frac{1}{\rho(t'+\tau)}\, p(t'+\tau)_{,i}$ Eq. (6.3) becomes:

$$\left[u_i' u_i \right]_{,\tau} + u_i' u_{j}\, u_{i,j} = -u_i' P_i - f\varepsilon_{i3k}\, u_i' u_k + u_i' F_i . \qquad (6.4)$$

Applying the operation of ensemble averaging to Eq. (6.4), using Eq. (6.2), and letting u_i be the deviation $u_i'(t'+\tau)$, P_i be $P_i'(t'+\tau)$, and F_i be $F_i'(t'+\tau)$, we obtain:

$$\left[\langle u_i' (u_i^c + u_i^p + u_i) \rangle \right]_{,\tau} + \langle u_i' (u_j^c + u_j^p + u_j)(u_i^c + u_i^p + u_i)_{,j} \rangle =$$

$$- \langle u_i' (P_i^c + P_i^p + P_i) \rangle - f\varepsilon_{i3k} \langle u_i' (u_k^c + u_k^p + u_k) \rangle + \langle u_i' (F_i^c + F_i^p + F_i) \rangle .$$

Using the facts that during ensemble averaging the climatological mean and the periodic component are constants and that the ensemble averages of the deviations are zero, we have:

$$\left[\langle u_i' u_i \rangle \right]_{,\tau} + \langle u_i' u_j u_{i,j} \rangle + \langle u_i' u_{i,j} \rangle \langle u_j^c + u_j^p \rangle$$

$$+ \langle u_i' u_j \rangle (u_i^c + u_i^p)_{,j} =$$

$$- \langle u_i' P_i \rangle - f\varepsilon_{i3k} \langle u_i' u_k' \rangle + \langle u_i' F_i \rangle . \qquad (6.5)$$

We assume all the functions in Eq. (6.5) to be second order stationary. Then the following covariances exist

$$R_{ij}(\tau) = R_{u_i' u_j}(\tau) = \langle u_i(t')\, u_j(t'+\tau) \rangle ,$$

$$R_{u_i' u_{i,j}}(\tau) = \langle u_i(t')\, u_{i,j}(t'+\tau) \rangle ,$$

$$R_{u_i' P_i}(\tau) = \langle u_i(t')\, P_i(t'+\tau) \rangle ,$$

$$R_{u_i' F_i}(\tau) = \langle u_i(t')\, F_i(t'+\tau) \rangle ,$$

$$R_{u_i' u_j u_{i,j}}(\tau) = \langle u_i(t')\, u_j(t'+\tau)\, u_{i,j}(t'+\tau) \rangle .$$

Eq. (6.5) may then be expressed in the form

$$R_{ii}(\tau)_{,\tau} + R_{u_i' u_j u_{i,j}}(\tau) + (u_j^c + u_j^p)\, R_{u_i' u_{i,j}}(\tau) \qquad (6.6)$$

$$+ (u_i^c + u_i^p)_{,j}\, R_{ij}(\tau) = -R_{u_i' P_i}(\tau) - f\varepsilon_{i2j}\, R_{ij}(\tau) + R_{u_i' F_i}(\tau).$$

Further we assume the existence of the following transform pairs (see e.g. Eq. (2.9))

$$R_{ij}(\tau) = \int_{-\infty}^{\infty} S_{ij}(\omega)\, e^{i\omega\tau}\, d\omega$$

$$S_{ij}(\omega) = \frac{1}{2\pi}\int_{-\infty}^{\infty} R_{ij}(\tau)\, e^{-i\omega\tau}\, d\tau\,. \tag{6.7}$$

$$R_{u_i' u_{i,j}}(\tau) = \int_{-\infty}^{\infty} S_{u_i' u_{i,j}}(\omega)\, e^{i\omega\tau} d\omega$$

$$S_{u_i' u_{i,j}}(\omega) = \frac{1}{2\pi}\int_{-\infty}^{\infty} R_{u_i' u_{i,j}}(\tau)\, e^{-i\omega\tau} d\tau\,, \tag{6.8}$$

$$R_{u_i' P_i}(\tau) = \int_{-\infty}^{\infty} S_{u_i' P_i}(\omega)\, e^{i\omega\tau} d\omega$$

$$S_{u_i' P_i}(\omega) = \frac{1}{2\pi}\int_{-\infty}^{\infty} R_{u_i' P_i}(\tau)\, e^{-i\omega\tau} d\tau\,, \tag{6.9}$$

$$R_{u_i' F_i}(\tau) = \int_{-\infty}^{\infty} S_{u_i' F_i}(\omega)\, e^{i\omega\tau}\, d\omega$$

$$S_{u_i' F_i}(\omega) = \frac{1}{2\pi}\int_{-\infty}^{\infty} R_{u_i' F_i}(\tau)\, e^{-i\omega\tau}\, d\tau\,, \tag{6.10}$$

$$R_{u_i' u_j u_{i,j}}(\tau) = \int_{-\infty}^{\infty} S_{u_i' u_j u_{i,j}}(\omega)\, e^{i\omega\tau}\, d\omega$$

$$S_{u_i' u_j u_{i,j}}(\omega) = \frac{1}{2\pi}\int_{-\infty}^{\infty} R_{u_i' u_j u_{i,j}}(\tau)\, e^{-i\omega\tau} d\tau\,, \tag{6.11}$$

$$\frac{\partial R_{ij}(\tau)}{\partial \tau} = \int_{-\infty}^{\infty} i\omega\, S_{ij}(\omega)\, e^{i\omega\tau}\, d\omega$$

$$i\omega S_{ij}(\omega) = \frac{1}{2\pi}\int_{-\infty}^{\infty} \frac{\partial R_{ij}(\tau)}{\partial \tau}\, e^{-i\omega\tau}\, d\tau\,, \tag{6.12}$$

where Eq. (6.12) is obtained from Eq. (6.7) and we assume the operation to be valid.

Now we multiply Eq. (6.6) by $\frac{1}{2\pi} e^{-i\omega\tau}$ and integrate with respect to τ:

$$i\omega S_{ii}(\omega) + S_{u_i' u_j u_{i,j}}(\omega) + (u_j^C + u_j^P)\, S_{u_i' u_{i,j}}(\omega) + (u_i^C + u_i^P)_{,j}\, S_{ij}(\omega) = -S_{u_i' P_i}(\omega) - f\varepsilon_{i3j}\, S_{ij}(\omega) + S_{u_i' F_i}(\omega)\,. \tag{6.13}$$

Using the equations analogous to Eq. (2.6), i.e. :

$$S_{ij}(\omega) = Co_{ij}(\omega) + i\, Q_{ij}(\omega)\,,$$

we can split Eq. (6.13) up into two equations

$$0 = -Co_{u_i' u_j u_{i,j}}(\omega) - (u_j^C + u_j^P)\, Co_{u_i' u_{i,j}}(\omega) - (u_i^C + u_i^P)_{,j}\, Co_{ij}(\omega) - Co_{u_i' P_i}(\omega) - f\varepsilon_{i3j}\, Co_{ij}(\omega) + Co_{u_i' F_i}(\omega) \tag{6.14}$$

$$\omega S_{ii}(\omega) = -Q_{u_i' u_j u_{i,j}}(\omega) - (u_j^C + u_j^P)\, Q_{u_i' u_{i,j}}(\omega) - (u_i^C + u_i^P)_{,j}\, Q_{ij}(\omega) - Q_{u_i' P_i}(\omega) - f\varepsilon_{i3j}\, Q_{ij}(\omega) + Q_{u_i' F_i}(\omega) \tag{6.15}$$

Using the relations from Eq. (2.10), for the Coriolis term in Eq. (6.14) we find:

$$-f\varepsilon_{i3j}\, Co_{ij}(\omega) = -f(-Co_{12}(\omega) + Co_{21}(\omega)) = 0$$

and in Eq. (6.15):

$$-f\varepsilon_{i3j}\, Q_{ij}(\omega) = -f(-Q_{12}(\omega) + Q_{21}(\omega)) = 2f\, Q_{12}(\omega)$$

From Eq. (6.15) we see that the average spectral density of kinetic energy multiplied by frequency is given by a sum of quadrature spectra. Because a quadrature spectrum gives a measure of a 90° out-of-phase relationship between the variables concerned, such an out-of-phase relationship must be essential for the shape of $S_{ii}(\omega)$.

From the previously quoted publications we know that a similar analysis in wave number space leads to a spectral equation relating the time rate of changes of the kinetic energy spectrum to a sum of cospectra, whereas we see that in the frequency domain the cospectral equation gives a balance among various cospectra.

Our interest is centered on the shape of $S_{ii}(\omega)$, for which reason only Eq. (6.15) will be further treated (for discussion of the implications of the cospectral equations see W.C. Chiu (1970)).

The signs of the quadrature terms are dependent on the convention used in the definition of the quadrature spectral tensor Eq. (2.6). If the spectral calculations are performed in the former traditional way using the covariances, the signs depend on which function is "leading" and which function is "lagging", because in general $R_{ij}(\tau) \neq R_{ij}(-\tau)$. Using the Fast Fourier Transform procedure, $Q_{u_i u_j}(\omega)$ is calculated with the right sign if y(l), in Eq. (4.1a), is defined as

$$y(l) = u_i(l) + i\, u_j(l) .$$

Thus the placing of the marks "," in Eq. (6.15) is significant for the signs on the right-hand side. Interchanging the marks causes all the quadrature spectra to change sign, but it is not obvious from the equation itself why we also have to change the sign on the left-hand side. This comes from Eq. (6.6) and from the fact that $R_{ii}(\tau)_{,\tau}$ is an odd function because $R_{ii}(\tau)$ is an even function.

6.3. Discussion of the Spectral Equation

To make the meaning of Eq. (6.15) clear let us repeat our main assumption: The atmospheric motions are stationary and because of the stationarity we must require stationary boundary conditions, hence there must be a balance between energy fed into the system and energy extracted from the system. Undertaking to find out how the flow field organizes its kinetic energy, we perform, with the same boundary conditions (same in a statistical sense), an infinite number of experiments, each carried out in the infinite four-dimensional space-time space, and measured along the time axis. Making the ensemble average of the spectral density of the kinetic energy, we find that this can be expressed as a sum of quadrature spectral densities, i.e. the shape of $S_{ii}(\omega)$ multiplied by ω is determined by a 90° out-of-phase relationship between various pairs of the variables.

For obvious reasons we have no information about the time rate of change of the spectrum, as is the case when the three-dimensional wave number space is considered where time is kept fixed during the Fourier transformation. The difficulties encountered in the interpretation of the various terms in Eq. (6.15) are perhaps even greater than those experienced in wave number space, and the reason for going through the whole mathematical exercise is that our measurements apply to one of the interesting terms in the equation: $2f\mathrm{Q}_{12}(\omega)$. But let us first shortly consider the other terms:

$Q_{u_i' u_j u_{i,j}}(\omega)$ is the effect of an out-of-phase relationship between the *fluctuating momentum*, u_i', and the *advection of fluctuating momentum* by the fluctuating motion $u_j u_{i,j}$.

$(u_i^c + u_i^p)_{,j}\, Q_{ij}(\omega)$ and $(u_j^c + u_j^p)\, Q_{u_i' u_{i,j}}(\omega)$ arise from the interaction between the fluctuating motion and the mean motion. The first term depends on the product of the shear of the mean motion and an out-of-phase relation between the components of the fluctuating motion. The second term is the product of the mean motion and an out-of-phase relation between the fluctuation motion and the shear of the fluctuating motion.

$Q_{u_i', P_i}(\omega)$ and $Q_{u_i', F_i}(\omega)$ originate from out-of-phase relations between the fluctuation motion and the fluctuating density-pressure gradient terms and the accelerations caused by viscosity respectively. For further information on the implications of these five terms we refer to W.C. Chiu (1970).

6.3.1. The Influence of the Rotating of the Earth

The term $2f\mathrm{Q}_{12}(\omega)$ shows that the rotation of the earth influences the shape of the kinetic energy spectrum. However, the term originates from the Coriolis force which can neither destroy nor create energy, so the average total kinetic energy of the atmosphere, i.e. the average sum of the kinetic energy of the mean motions and the kinetic energy of the eddy motions, is independent of the rotation of the earth.

To get the energy of the mean motion, we multiply Eq. (6.1) by u_i and ensemble average. The contribution from the Coriolis term is $\langle f\varepsilon_{i3k} u_k u_i \rangle \equiv 0$, and from this follows that the energy of the eddy motions also is independent of the Coriolis forces. From Eq. (6.15) we have:

$$\int_0^{\infty} S_{ii}(\omega)\, d\omega = \int_0^{\infty} \frac{1}{\omega} \left[-Q_{u_i' u_j u_{i,j}}(\omega) - (u_j^c + u_j^p)\, Q_{u_i' u_{i,j}}(\omega) \right.$$
$$\left. - (u_i^c + u_i^p)_{,j}\, Q_{ij}(\omega) - Q_{u_i' P_i}(\omega) + 2f\mathrm{Q}_{12}(\omega) + Q_{u_i' F_i}(\omega) \right] d\omega .$$

Hence, from the discussion above

$$\int_0^\infty \frac{1}{\omega} Q_{12}(\omega)\, d\omega = \int_0^\infty Q_{12}(\omega)\, d\ln\omega \equiv 0 . \qquad (6.16)$$

$Q_{12}(\omega)$ is an antisymmetric function which gives $Q_{12}(\omega) \to 0$ for $\omega \to 0$ and from the theory and measurements of microturbulence we know $Q_{12}(\omega) \sim 0$ for $\omega > \sim 10^{-3}$ Hz. Figs. 25 and 26 show $Q_{12}(\omega)$ for Station Nord and the Risø Tower at 56m respectively. On both figures the tendency for the quadrature spectrum to go to zero for high frequencies is evident. Also to be noticed from both figures is the large widening of the confidence limits as low frequencies are approached. The Risø quadrature spectrum is positive for frequencies larger than 10^{-6} Hz and has a tendency to go towards negative values at lower frequencies. The fulfilment of Eq. (6.16) requires in this case that $Q_{12}(\omega)$ must be negative somewhere in the interval $0 < \omega < 10^{-6}$ Hz, but from our measurements we cannot say how and where. It is interesting to note that the high quadrature spectral densities are concentrated in the interval $10^{-6} < \omega < 10^{-4}$, i.e. on the cyclonic scale. However, this is not surprising; we know that this scale is connected with large rotating systems and further that rotating a wind vector creates and out-of-phase relation between the vector components. The really interesting point in this investigation lies in the comparison between the Risø and the Station Nord data. The quadrature spectrum from Station Nord (QSN) is quite different from the Risø quadrature spectrum (QR) on the synoptic scale where the tendency for QSN is to be either zero or negative, whereas the energy spectra for the two series are very similar.

Because of the deflecting nature of the Coriolis force we must expect it to exert a strong influence on the types of motion which the atmosphere follows and on the distribution of kinetic energy. How this force, arising from the rotation of the earth, influences $S_{ii}(\omega)$ is given by the product of the Coriolis parameter, f, and the quadrature spectrum, $Q_{12}(\omega)$, and this product is to be divided by the frequency ω. A natural way to estimate the explicit effects of the rotating of the earth on the kinetic energy distribution is then to plot the ratio $2fQ_{12}(\omega)/(\omega S_{ii}(\omega))$ versus ω (or $\ln\omega$). The kinetic energy spectrum, $S_{ii}(\omega)$, and the quadrature spectrum, $Q_{12}(\omega)$, are, in contrast to the cospectrum, $Co_{12}(\omega)$, independent of the orientation of the coordinate system; hence a rotation of the coordinate system as described in chapter 5 will not affect the ratio $2fQ_{12}(\omega)/(\omega S_{ii}(\omega))$.

Severe problems arise as $\omega \to 0$ because of the great uncertainty of the quadrature spectral estimates. Keeping this in mind and also the fact that the QR is evaluated from 10 years' of data whereas the QSN only covers a summer period, we have taken the single spectral estimates, formed the ratios and smoothed them with the usual smoothing procedure. The results are displayed in figs. 27 and 28. It is evident that the Coriolis effects are of extreme importance for the Risø energy spectrum, especially on the synoptic scale, whereas the plotted ratio for Station Nord fluctuates greatly showing a slight tendency as indicated by the broken line. Much cannot be deduced from this graph; the point to be made here is that whereas the energy spectra show much the same distribution of kinetic energy for the two stations, we must, from the plots on figs. 27 and 28, expect the various terms in Eq. (6.15) to exert quite different influences on the two spectra. More data are needed from Station Nord to get statistically reliable results, fortunately such data will be available in the future from the previously mentioned automatic station.

We feel that an analysis along the lines indicated here may be advantageous; thus in addition to our recommendation for calculating when possible the component spectra rather than the speed spectra, we recommend the calculation of the ratio investigated above. Using a complex Fast Fourier Transform, no additional work is required because, in addition to the u and the v spectra, also the co and the quadrature spectra are calculated.

With the component spectra, the quadrature spectra and the ratio from sufficiently long time series from various locations on earth, much more knowledge can be acquired about the structure and causes of large scale atmospheric turbulence than is the case when just speed spectra are calculated.

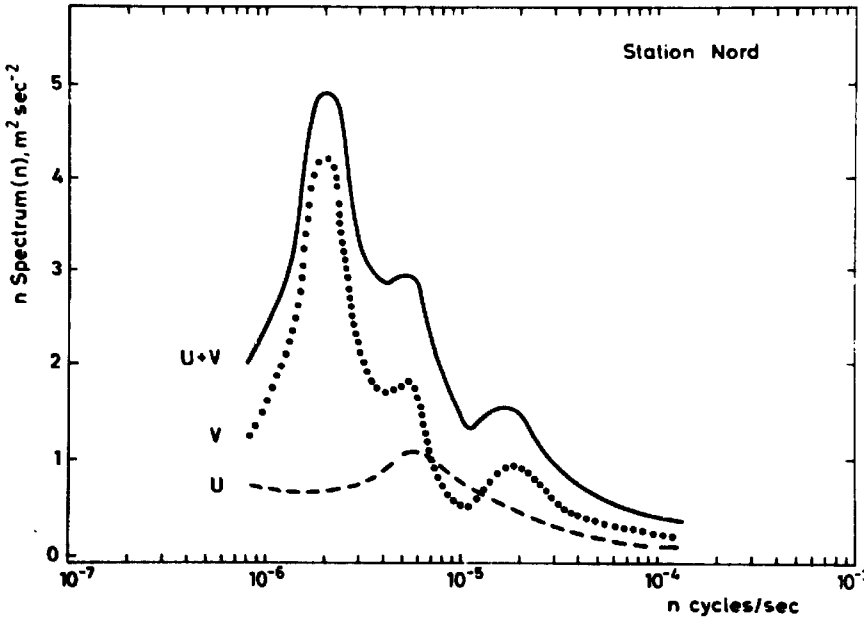

Fig. 24. Component spectra measured at Station Nord, Greenland, in the summer of 1972.

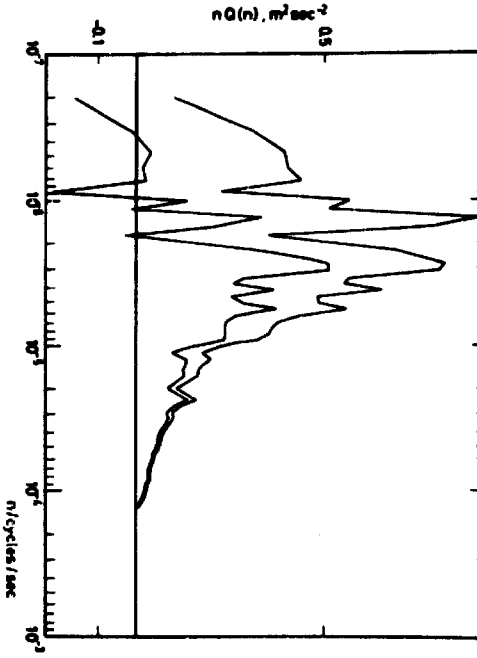

Fig. 25. Quadrature spectrum. Risø 1958-67, 56 m. The plotted curves are the confidence limits, cf. section 4.4.

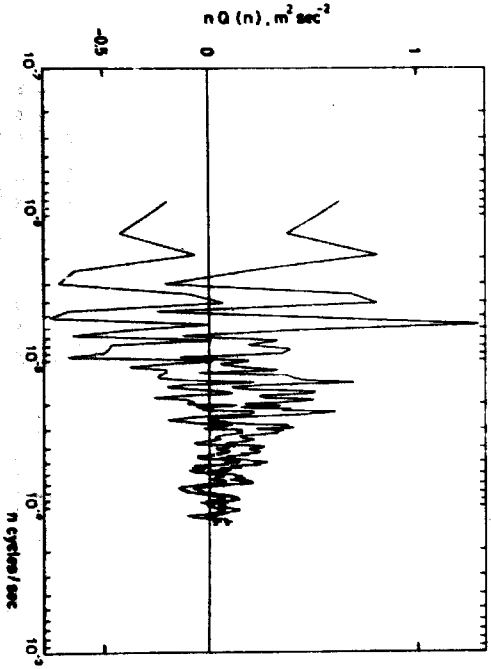

Fig. 26. Quadrature spectrum. Station Nord, Greenland, the summer of 1972. The plotted curves are the confidence limits, cf. section 4.4.

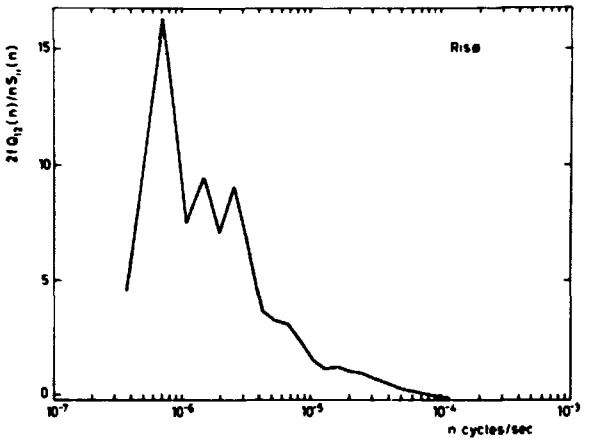

Fig. 27. Curve showing the explicit effect of the rotating of the earth on the energy spectrum measured at Risø 1958-67 at 56 m.

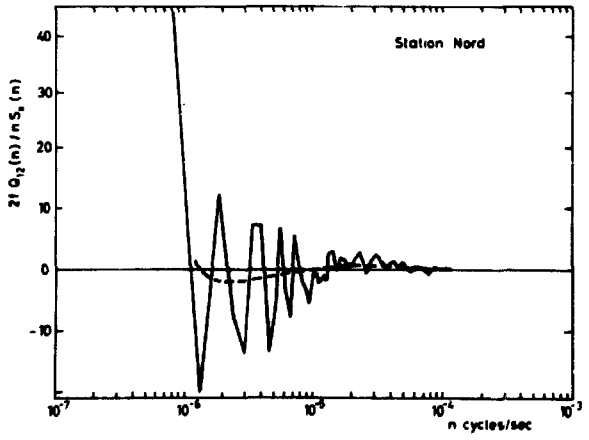

Fig. 28. Curves showing the explicit effect of the rotating of the earth on the energy spectrum measured at Station Nord, Greenland, the summer of 1972. The unbroken line is calculated, the broken line is fitted by eye.

7. DAILY VARIATION OF METEOROLOGICAL ELEMENTS

This chapter concerns the response of the lowest hundreds of metres of the planetary boundary layer to the diurnal variation of insolation. The reason for this discussion is two-fold: firstly, the daily cycle introduced in the wind field causes lines in spectra which otherwise are considered continuous, hence a special investigation is necessary. Secondly, there is no general agreement about the description of the dynamics of this layer and we believe that the Risø Tower data may add to the knowledge of the behaviour of this layer. The measured daily variations of the meteorological elements, such as wind speed, wind direction, and temperature, exhibit characteristics which in general are consistent with those found elsewhere over quite different terrain. However, in many circumstances the data reveal an exceptionally and unexpectedly large turning of the wind with height above the ground.

Because of the importance of wind direction shear in many applications, e.g. the evaluation of diffusion from stacks, an attempt is made to model the phenomenon numerically. The final formulation of the model and the problems encountered in the numerical treatment of the equations have not yet been fully solved, and although preliminary results show agreement between model and observation we have decided to present the subject in a future report. Instead, phenomenological descriptions are attempted here by means of solutions to equilibrium problems.

7.1. The Planetary Boundary Layer

Solar energy arrives at the top of the atmosphere at an average rate of 0.5 cal cm^2 $min.^{-1}$. S. L. Hess (1959) estimates for the Northern Hemisphere that the average solar radiation absorbed at the ground is approximately 50% of this amount, 35% is reflected and the rest is absorbed in the troposphere, mostly by water vapour and dust. Thus the air of the troposphere receives practically no direct heat from solar radiation whereas the temperature of the soil surface may vary greatly due to fluctuations in the solar radiation flux, the most significant reason for variations being the rotation of the earth.

When the ground becomes warmer than the adjacent air, heat moves from ground to air. No air velocities exist right at ground level and the transfer of heat must take place by molecular conduction down a very strong temperature gradient. Higher up transfer takes place through forced-convection where heat is transported by almost mechnical turbulence. Further up the amount of turbulence induced by buoyancy is increased and less turbu-

lence is mechanically induced. The temperature variation at the ground then gives rise to variations of the intensity of the exchange of heat and momentum between adjacent air layers causing variations in the vertical wind velocity and temperature profiles.

Thus a layer of the atmosphere is exposed to both a thermal and a dynamical influence from the ground, the latter being caused by the adhering of the air to the surface. This layer is called the planetary boundary layer and its height varies from approximately 1 km to 2 km. What especially characterizes the planetary boundary layer is that the profiles of the meteorological elements are mutually dependent. For obvious reasons, despite the complex nature of even the simplest problems, it has become one of the most important goals in atmospheric physics to clarify the spatial and time-variation laws of the fields of the meteorological elements in the planetary boundary layer.

7.2. The Boundary Layer Equations

A complete representation of the daily variation of the parameters characterizing the boundary layer could be obtained from the solution of the entire system of governing equations, which contains three equations for radiative energy transfer - in addition to the second law of mechanics, the conservation law of the mass of air and water vapour, the conservation law for transformation of energy, and the equation of state. A discussion of this system of ten equations is given in D. L. Laikhtman (1964) which shows that even a formulation of the problem proves very difficult and one has to rely heavily on qualitative and phenomenological descriptions.

In our further discussions we shall focus our attention on the momentum equation for the horizontal wind vector Eq. (6.1) and neglect the viscous term:

$$u_{i,t} + u_j u_{i,j} = -\frac{1}{\rho} p_{,i} - f\varepsilon_{i3k}u_k \,. \tag{7.1}$$

Further the Reynolds convention is used. Let $\langle u \rangle$ denote the sum of the steady mean and the periodic mean. Averaging Eq. (6.1), we obtain the equations for the mean motions

$$\langle u_i \rangle_{,t} + \langle u_j \rangle \langle u_i \rangle_{,j} = -\frac{1}{\rho}\langle p \rangle_{,i} - \langle u_i' u_j' \rangle_{,j} - f\varepsilon_{i3k}\langle u_k \rangle \,.$$

Neglecting the horizontal variation of the turbulent fluxes, as compared to the vertical variation, and neglecting the horizontal variation in the mean flow we have (dropping the averaging signs):

$$\frac{\partial u_1}{\partial t} = -\frac{1}{\rho}\frac{\partial p}{\partial x_1} - \frac{\partial}{\partial x_3}(u_1' u_3') + f u_2$$

$$\frac{\partial u_2}{\partial t} = -\frac{1}{\rho}\frac{\partial p}{\partial x_2} - \frac{\partial}{\partial x_3}(u_2' u_3') - f u_1 \,. \tag{7.2}$$

Introducing the geostrophic wind

$$\underline{G} = (u_g, v_g) = \left(-\frac{1}{f\rho}\frac{\partial p}{\partial x_2}, \frac{1}{f\rho}\frac{\partial p}{\partial x_1}\right) \tag{7.3}$$

and the stress vector $\tau = (\tau_x, \tau_y) = -\rho\,(u_1' u_3', u_2' u_3')$, we get (using the u, v, and z notation):

$$\frac{\partial u}{\partial t} = \frac{\partial \tau_x/\rho}{\partial z} + f(v - v_g)$$

$$\frac{\partial v}{\partial t} = \frac{\partial \tau_y/\rho}{\partial z} - f(u - u_g) \,. \tag{7.4}$$

To proceed further it is necessary to establish a relation between the shear stress vector, $\underline{\tau}$, and the velocity field. Unfortunately such a relationship cannot be found from first principles and must be established in an empirical manner. By analogy to Newton's formula for a laminar flow

$$\tau_x = \rho\nu \frac{\partial u}{\partial z} \,,$$

the Boussinesq eddy viscosity is used for turbulent flows

$$\tau_x = \rho K_{M_x} \frac{\partial u}{\partial z} \,, \tag{7.5}$$

$$\tau_y = \rho K_{M_y} \frac{\partial v}{\partial z} \,.$$

K_M is also called the austausch coefficient, the eddy exchange coefficient for momentum, or just the eddy diffusivity.[1] K_{M_x} and K_{M_y} are not necessarily equal, but almost without exception this is always assumed. There are two possibilities for proceeding from this definition. Either K can be prescribed by some empirical function of height and time, or it can be expressed in terms of other unknowns which relate K in some way to the mean flow. The second possibility is commonly connected with Prandtl's mixing length theory and the Monin-Obukhow similarity theory; K is then given as a function of height and stability. The variation of the mixing length has to be given before-

[1] Because the introduction of a K-profile is essentially tantamount to parameterization of the effects of small scale atmospheric turbulence on large scale fields, the usefulness of the K-theory is very closely connected to the existence of a spectral gap as discussed in chapter 5.

hand, and a formula suggested by Blackadar (1962) has been used quite successfully in modelling stationary wind fields. Another characteristic length, which can be related to eddy viscosity, has been suggested by N. E. Busch and H. A. Panofsky (1968). This length is the wavelength where the energy spectrum of the vertical velocity component has its maximum in a $n\,F(n)$ versus $\ln n$ representation. The behaviour of this length appears to be consistent with that of the mixing length.

The predicted profiles on fig. 4 have essentially been obtained by using these two lengths.

Here we do not wish to proceed further with the mixing length theory, and we turn our attention to the first of the possibilities mentioned above, a prescription of the K profile.

Introduction of Eq. (7.5) into Eq. (7.4) yields

$$\frac{\partial u}{\partial t} = \frac{\partial}{\partial z}\left(K \frac{\partial u}{\partial z}\right) + f(v - v_g)$$

$$\frac{\partial v}{\partial t} = \frac{\partial}{\partial z}\left(K \frac{\partial v}{\partial z}\right) - f(u - u_g), \qquad (7.6)$$

where u, v, k, u_g, and v_g are functions of time and height, and the boundary conditions are

$$u(z_o, t) = v(z_o, t) = 0 \quad ,$$

$$u(z > z_g, t) = u_g(z > z_g, t),$$

$$v(z > z_g, t) = v_g(z > z_g, t),$$

When the wind field is considered to contain a daily cycle, the conditions of periodicity are:

$$u(z,t) = u\left(z, t + \frac{2\pi}{\Omega}\right)$$

$$v(z,t) = v\left(z, t + \frac{2\pi}{\Omega}\right) \quad .$$

(z_o is roughness length, Ω is the angular velocity of the earth's rotation, and z_g is a height of the same order as that of the planetary boundary layer).

7.3. Analytical Solution to the Equations

In the simplest case with stationary conditions, constant eddy diffusivity and height-independent geostrophic wind, the solution to Eq. (7.6) can be found analytically, yielding the well-known Ekman's spiral. Under the same assumptions but with K given as simple analytic functions, other mathematical spirals have been found, e.g. the Rossby spiral (see e.g. H. Lettau, 1970). In the non-stationary case, still with constant geostrophic wind with height, an analytical solution has been given by D. L. Laikhtman (1964) for a K-variation of the form

$$K(z,t) = k(z)(1 + B\cos \Omega t) \qquad (7.7)$$

$$k(z) = \begin{cases} k_o + k\,z & \text{for } z < h \\ k_o + k\,h & \text{for } z \geq h \end{cases},$$

where B, k_o, k_1, and h are constants. Even for such a simple K profile, the mathematical calculations become rather cumbersome and an interpretation of the solution, in this case infinite summations of products of expansions in Bessel and Neuman functions, is difficult to carry out.

C. M. Sheih (1972) presents a solution for the same case except that K is not a function of height. Although his solution seems usable, the assumptions necessary for the mathematical treatment (u and v constant and a step discontinuity in the K profile for $z = 0$) considerably reduce the usefulness of the solution for our purpose.

7.4. Numerical Modelling of the Planetary Boundary Layer

From the discussion above, and a survey of the relevant literature, one is led to the generally accepted fact that at present the most rewarding method to be used in the investigation of the relative importance of the different external factors and internal processes in determining the behaviour of the planetary boundary layer, is numerical integration of the governing equations by finite-difference methods and deductions from the results of the integration.

However, not many of the external and internal factors have to be specified before one gets hopelessly stuck in the complexities of boundary layer phenomena, and only through recourse to parameterization can useful deductions be made.

One of the commonest applications of numerical modelling is the study of a single effect, for instance a transient in the geostrophic wind. After a first molding of the numerical model, experiments have to be carried out on the basic of deductions from the model. The model is then adjusted to the experience gained from the experiments being used, new experiments are made and so on. Indeed, comparisons between models and experimental data are the only way to justify models in atmospheric science.

The problem we are facing differs only slightly from what we have mentioned above; we wish to study and explain some characteristic features found in the data from an experiment that has been carried out during ten years.

At this point we advise the reader to look at fig. 31 (actually 36 figures) and its explanation.

Since our aim is to investigate diurnal variations of meteorological elements, an obvious handling of the data is to separate irregular fluctuations from the daily ones by grouping the records according to the time of day and by averaging each hour separately. Because of the yearly variations, the significance of which is indicated on figs. 1 and 19, the procedure above is far too crude, the data at least must be grouped separately for each month as in fig. 31. This grouping is then a compromise between the desire for statistical reliability and the desire to distinguish different features in the daily variations with the possibility of explaining these features through their yearly variations. Although confidence limits ate not shown on fig. 31, the statistics are quite good; to every hourly point plotted there pertain about 300 observations.

The following six points display a simple strategy which should make it possible to achieve our aim:

1) Grouping and averaging the data (explained above)

2) Close study of the results of the grouping and averaging. Single features are picked out and it is investigated to what an extent they can be explained through the use of solutions to equilibrium problems. If such an investigation is carried out with success, the considered external factors or internal processes are subjected to a quantitative description by the use of the data.

3) A numerical model is set up based on the boundary layer equations Eq. (7.6) with the appropriate approximations, parameterizations, and closure chosen with respect to the evidence obtained under (2).

4) Comparison between model and observations. Adjustment of the model and perhaps also of the grouping and averaging procedure.

5) Performance of, if possible, short-duration experiments to verify crucial points in the model such as the paramerization of small-scale turbulence and of radiation.

6) Documentation of the applicability of the model.

It is clear that feedback occurs between various points.

As previously mentioned, the numerical model will not be investigated here, and only point (2) is investigated in the rest of this report.

7.5. Deductions from Measured Mean Profiles Using the Principle of Equilibrium Motion

The most obvious feature to be observed from fig. 31 is the increase in wind speed near the ground in the daytime. To be specific, let us follow the displayed variations in the month of October.

Early in the morning before sunrise the temperature increases with height and decreases with time because heat is conducted to the cool ground, which in turn loses heat through outgoing longwave radiation; the time rate of change in temperature is almost constant from midnight till sunrise. The sun rises between 6.30 and 7.30 a.m., the ground is heated, and heat moves from it to the adjacent air, thus creating an unstable air layer. Because of the significant vertical uplift velocities of the warm thermals, the whole of the layer considered registers the heating in the course of a few minutes.

The convection causes the wind speed to increase at all heights because the ascending bodies of air originating at low levels are replaced by descending air parcels from higher levels which tend to bring down with them the higher speeds prevalent at those levels. At 8.00 the mixing becomes so effective in thelowest 90 m that the momentum transport from the layer above 123 m lags behind the momentum used to speed up the lower layers and the momentum lost through the surface frictional drag. The result is a decrease of speed in the layer above 96 m. At 10.00 the momentum transport through the top becomes sufficient to support the increase of speed at all heights; at 13.00 the temperature difference between top and bottom, the mixing, and the speed in the layer up to 72 m reach their maxima during the diurnal cycle. From then on the heat lost from the ground owing to longwave radiation and conduction exceeds the heat gained through the incoming shortwave radiation; the ground cools and reaches a temperature lower than the adjacent air. This causes the heat flux to reverse and a stably stratified air

layer near the ground is thus created. The Rynolds stresses weaken, resulting in a decoupling of the layers from above, which now start to speed up almost entirely under the influence of the pressure and the Coriolis forces.

The velocity of the air moving in equilibrium with the pressure gradient and the Coriolis force is called the geostrophic wind. This was introduced in Eq. (7.3) and can be found from Eq. (7.2) putting the derivative, with respect to time, and the frictional term equal to zero.

Hence the wind described above may be considered as a wind which during the day is disturbed by frictional retardation from its geostrophic equilibrium value. With the rapid diminishing of the eddy viscosity about sunset, the decoupled air layer begins to move towards a state of equilibrium. The result is a wind oscillating around its geostrophic value with a period of half a pendulum day (14 1/2 hours at 57°), a movement sometimes called initial inertial oscillations. This can be found from Eq. (7.4) if the frictional term is omitted, and if the wind is considered as constant with height, which allows the partial derivative to be replaced by a substantial derivative. The solution reveals that a vector must be added to the actual wind vector at the initial time. While maintaining a constant magnitude, this vector rotates in the clockwise direction with a period of half a pendulum day.

It is now obvious how the increase in wind speed at 123 m at 16.00 and at 7 m at 18.00 should be explained. Further evidence is given by the displayed turning of the wind vector with height: at 16.00 the angle between the wind vectors at 7 m and at 123 m is almost zero, but the angle is increasing and reaches a value of 12 degrees around midnight. The increase of the wind speed with height and with time is continued up to heights around 300 to 1000 m where a local maximum on the wind speed profile may occur sometimes. Actually this maximum may be so large that it bears resemblance to a jet; thus it has been called the low-level jet. As Blackadar (1959) explains: "Unlike the jet stream which is situated at greater heights (10,000 to 15,000 metres) this low-level jet stream usually covers a wide horizontal area. Rather than looking like a river, it is as if a sheet of rapidly moving air was sandwiched between slower layers above and below".

The strong wind shear that is generated occasionally causes turbulence, and hereby a weak but significant downward loss of momentum, which tends to smooth out the oscillations. This is demonstrated on the figure where the wind speeds are almost constant at all heights from midnight to sunset.

In the introduction to this chapter it was mentioned that the measured

daily variations of the wind speed, wind direction, and temperature exhibit characteristics which in general are consistent with those found at other locations over quite different terrain (see e.g. F. Fiedler, 1971, where two figures are given which show the daily variation of the wind velocity at 2, 5, 10, 20, and 50 m in January and June, near Munich). The large turning of the wind with height above the ground is very exceptional, but we find that the whole collection of 36 figures gives an outstanding portrait of boundary layer behaviour. The above treatment is, of course, not restricted to the month of October; on the contrary, the amplification or diminishing of the various effects throughout the year give support to the theories advanced.

To get an idea of the causes of the large turning, we note that around noon in the months with large insolation the mixing is so strong in the lowest hundred metres that no turning is to be expected. Fig. 31 reveals that in the months from March to October the turning is actually negative. We have good reasons to believe that this is not caused by instrument or alignment errors. Quite naturally our thoughts are directed towards an explanation by horizontal inhomogeneities in the pressure field, these again being caused by horizontal inhomogeneities in the thermal properties of the surface. Fig. 3 demonstrates that in a section of approximately 270° the wind has travelled over water before reaching the Risø Tower, and to this can be added that the most common wind direction is west-southwest. From March to October the surface temperature of the ground will be higher around noon than the temperature of the water. For the rest of the day the opposite is the case (unfortunately only a one-year record of water temperature is available, but close inspection of this record makes us feel sure on this point).

On figs. 29 and 30 are displayed for every month the minimum and the maximum angle between the wind vectors at 123 m and 7 m, and the temperature difference between these two heights at the time when the angles were measured. It is obvious from the two figures that both angles contain a pronounced yearly cycle. The maximum negative turning occurs together with the maximum lapse rate in the month where the sun has maximum declination at culmination.

The maximum positive turning occurs in the same month, and at night when the temperature of the surface goes below the temperature of the water.

From elementary meteorological textbooks it is known that in a baroclinic atmosphere a horizontal temperature gradient causes a shear in

the geostrophic wind with height and this shear is given by the thermal wind equations

$$\frac{\partial v_g}{\partial z} = \frac{g}{fT}\frac{\partial T}{\partial x} + \frac{v_g}{T}\frac{\partial T}{\partial z}$$

$$\frac{\partial u_g}{\partial z} = -\frac{g}{fT}\frac{\partial T}{\partial y} + \frac{u_g}{T}\frac{\partial T}{\partial z} \qquad (7.8)$$

which are easily found from the geostrophic wind equations, the hydrostatic equation and the equation of state (T is the absolute temperature).

In the case considered the second terms on the right-hand side of both equations are an order of magnitude smaller than the first term and can be neglected. Let the wind blow from west to east and let $\partial T/\partial y \sim 0$. At night $\partial T/\partial x < 0$ and the wind will turn to the right with height; in the day $\partial T/\partial x > 0$ and the turning will be to the left, exactly what is observed.

The description above does not take frictional forces into account and therefore there is no need to further attempt to make quantitative arguments. What our analogy to the thermal wind has shown is the importance of including variations in the pressure field in the model, if that is to describe observed features properly.

Eq. (7.6) can be written in the form

$$\frac{\partial (u-u_g)}{\partial t} + \frac{\partial u_g}{\partial t} = \frac{\partial}{\partial z}\left(K\frac{\partial (u-u_g)}{\partial z}\right) + \frac{\partial}{\partial z}K\frac{\partial u_g}{\partial z} + f(v-v_g)$$

$$\frac{\partial (v-v_g)}{\partial t} + \frac{\partial v_g}{\partial t} = \frac{\partial}{\partial z}\left(K\frac{\partial (v-v_g)}{\partial z}\right) + \frac{\partial}{\partial z}K\frac{\partial v_g}{\partial z} - f(u-u_g). \qquad (7.9)$$

These equations, which have to be solved numerically, and the appropriate boundary conditions are the base of the model; $u_g(z, t)$, $v_g(z, t)$ and $K(z, t)$ have to be described beforehand. After comparisons between fields predicted by the model and observed fields, these three functions should be altered until comparisons are worked out satisfactorily. For instance, the model should yield significant information, such as that in the daytime of the months April to August a local maximum occurs in the wind profile somewhere between 72 and 123 m. Through this process much can be learned about phenomena on all scales in the boundary layer.

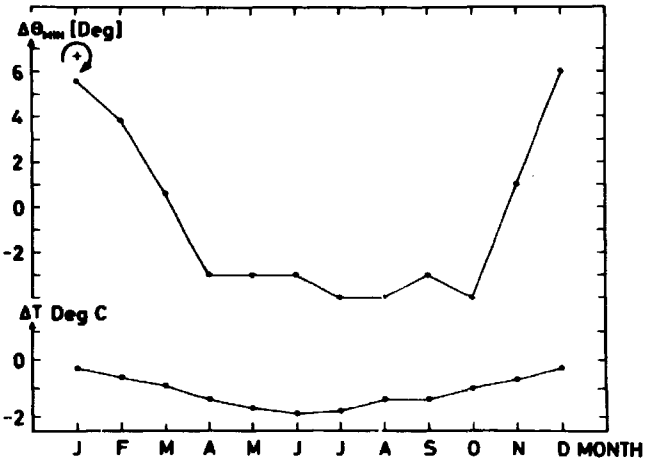

Fig. 29. Curves displaying for every month the minimum angle θ_{MIN} between the wind vectors at 123 m and 7 m, and the temperature difference between these two heights at the time when θ_{MIN} occurs.

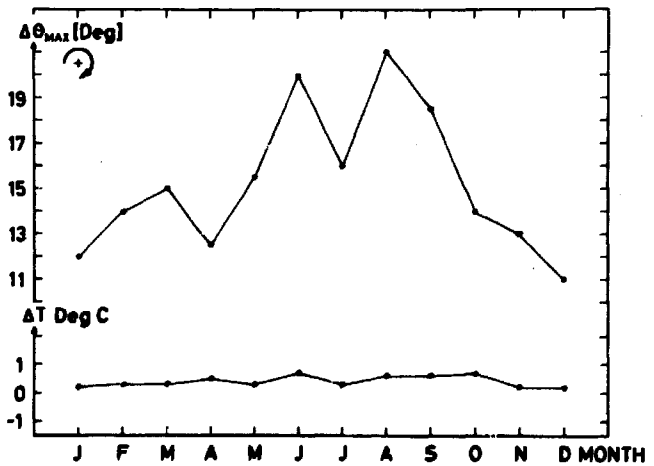

Fig. 30. As fig. 29 but with the maximum angle θ_{MAX}.

Fig. 31

For each month of the year the following 36 figures (called fig. 31) show the average daily variation, both in time and with height, of the temperature, the horizontal wind speed, and the turning of the horizontal wind vector as measured at the Risø Tower during the ten years 1958-67. Temperature, wind speed, and turning are shown in that sequence from top to bottom. The measure is the same on all axes through the year, but the placing of the zero point of the vertical axes for temperature and wind speed is changed from month to month.

Temperature: Curves for the 8 heights 2, 7, 23, 39, 56, 72, 96, and 123 m are shown. 2 m is indicated by ✱—✱ and 123 m by ⊟—⊟. It may be difficult to distinguish the curves of the intermediate heights especially at night. From April to October the temperature decreases through the whole 123 m layer by day which fact can be used to pick out a single height and follow it through the day. It is easy to distinguish stable from unstable situations on all figures.

Wind speed: Curves for the same heights as for temperature, except for 2 m where wind speed was not measured. 7 m is indicated by ✱—✱ and 123 m by ⊟—⊟. With minor exceptions the curves can easily be distinguished because in general the wind speed increases from bottom to top.

Turning: ✱—✱ indicates the angle between the horizontal wind vectors at 123 m and 7 m. ⊟—⊟ gives the angle between the vectors at 56 m and 7 m. Signs are used so that the angle is said to be positive if the vector turns clockwise with height. The curves should be visually smoothed before use - some of the peaks are due to the uncertainties in the calculations when $\Delta\theta$ is around 180°.

The following small sceme is inserted to facilitate the use of fig. 31:

The first day in the month of	Sunrise	Culmination	Declination at culmination	Sunset
Jan.	8.42	12.13	-23.03	15.45
Feb.	8.07	12.23	-17.17	16.40
Mar.	7.03	12.22	- 7.27	17.43
Apr.	5.43	12.14	4.41	18.46
May	4.29	12.07	15.11	19.46
June	3.36	12.07	22.06	20.40
July	3.33	12.13	23.06	20.54
Aug.	4.17	12.16	17.56	20.13
Sep.	5.16	12.10	8.10	19.02
Oct.	6.14	11.59	- 3.19	17.43
Nov.	7.18	11.53	-14.32	16.28
Dec.	8.17	11.59	-21.51	15.40

The time is Central European Time, i.e. Greenwich Mean Time plus one hour. To get the appropriate times for Risø 10 minutes should be added to the numbers above.

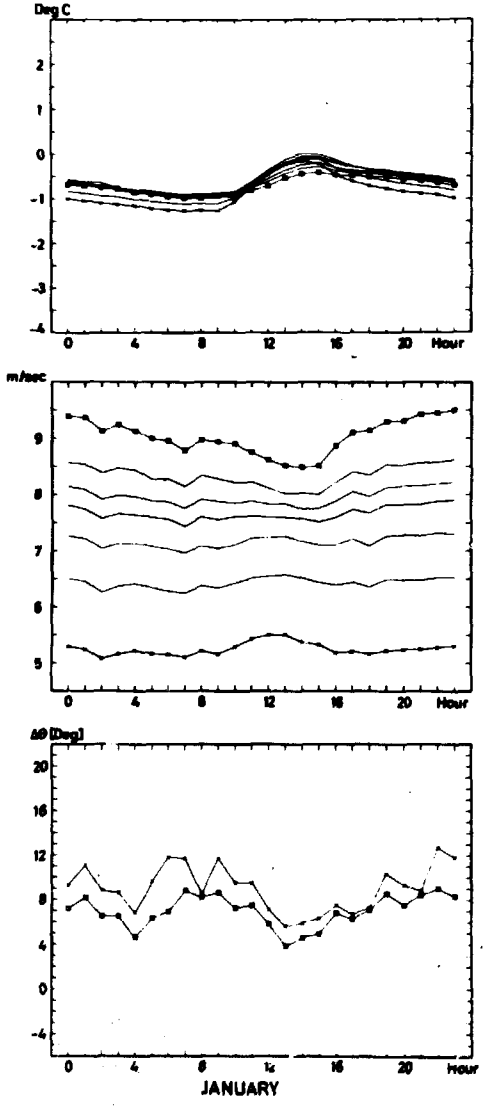

JANUARY

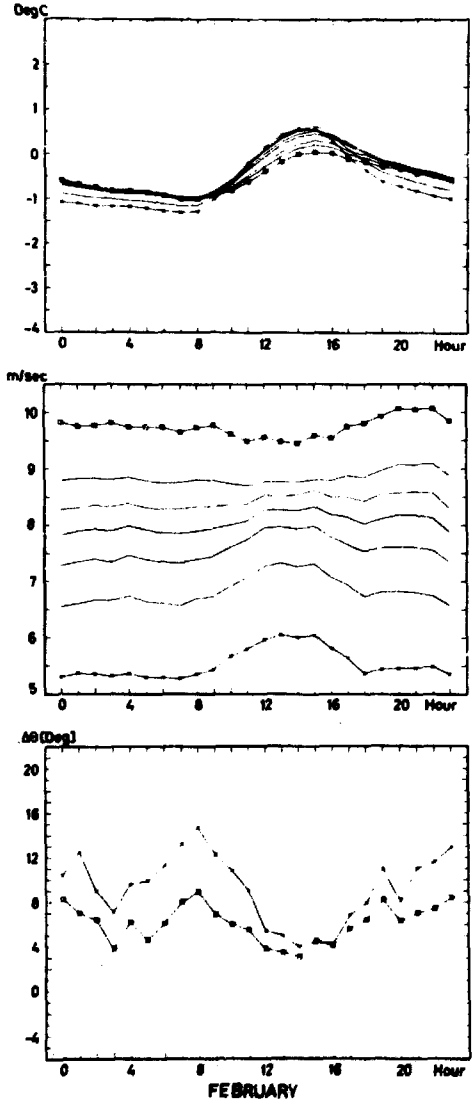

FEBRUARY

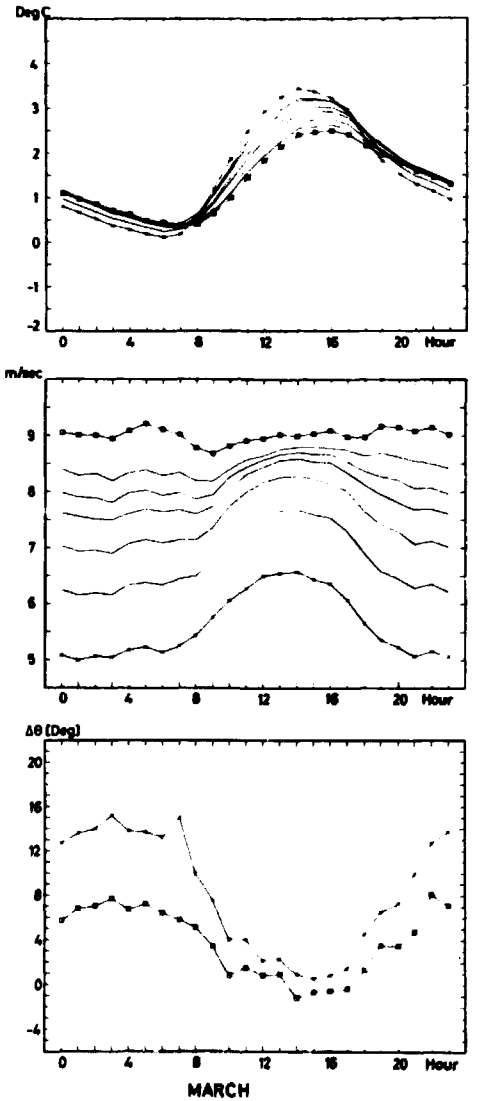
Deg C
m/sec
Δθ (Deg)
Hour
0
4
8
12
16
20

MARCH

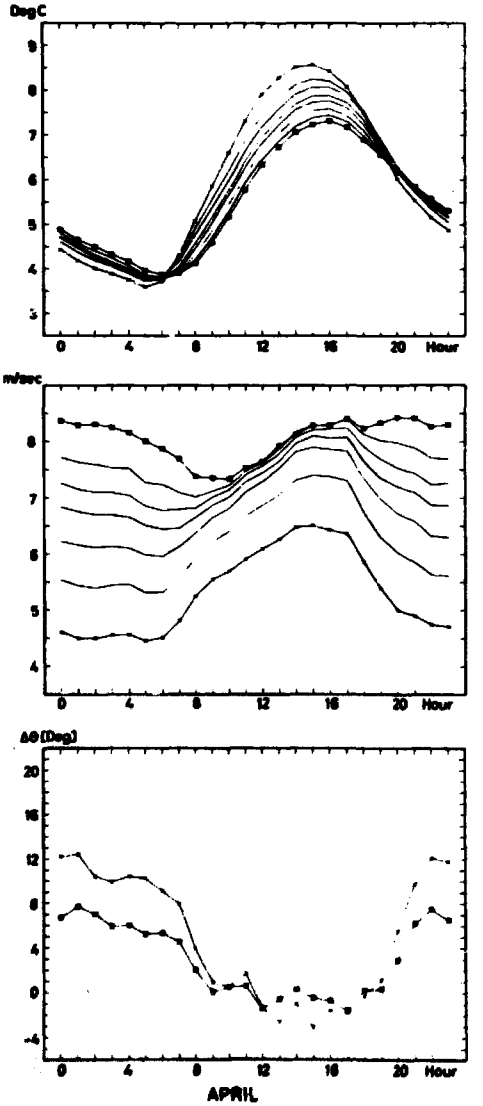
Deg C
m/sec
Δθ (Deg)
Hour
0
4
8
12
16
20

APRIL

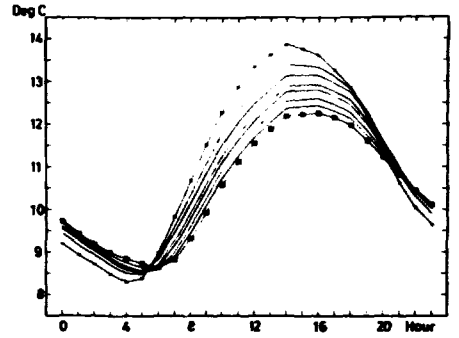
Deg C
14
13
12
11
10
9
8
0
4
8
12
16
20
Hour

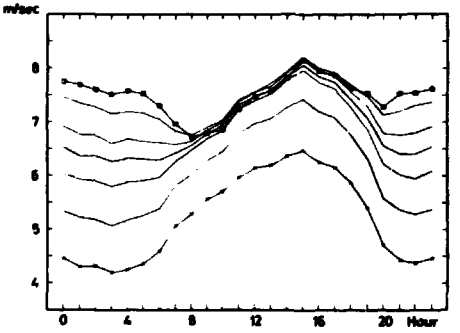
m/sec
8
7
6
5
4
0
4
8
12
16
20
Hour

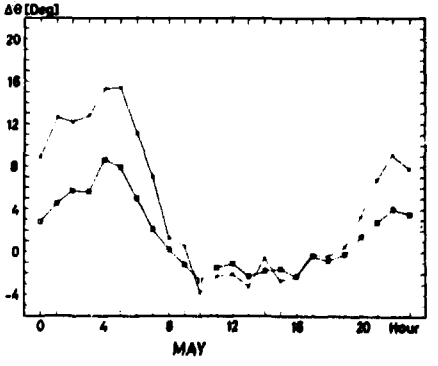
Δθ [Deg]
20
16
12
8
4
0
-4
0
4
8
12
16
20
Hour

MAY

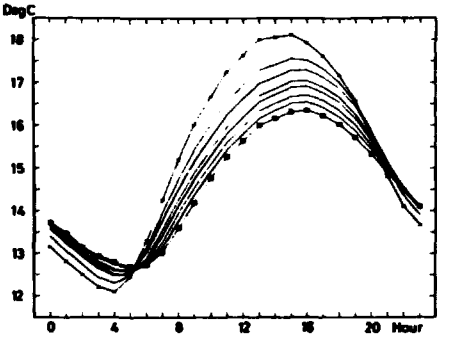
Deg C
18
17
16
15
14
13
12
0
4
8
12
16
20
Hour

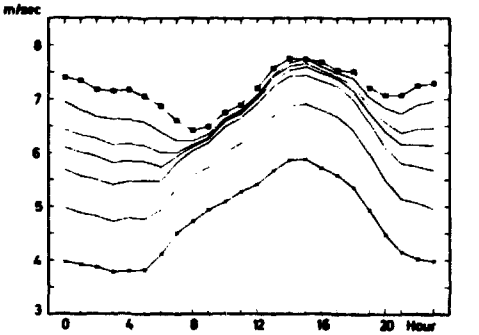
m/sec
8
7
6
5
4
3
0
4
8
12
16
20
Hour

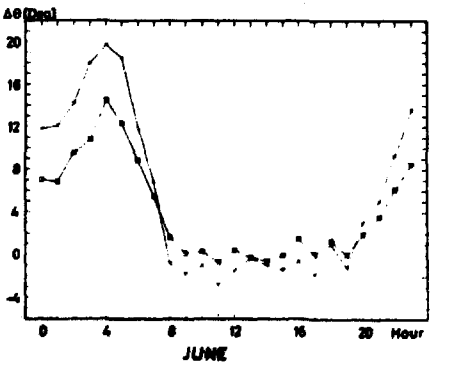
Δθ [Deg]
20
16
12
8
4
0
-4
0
4
8
12
16
20
Hour

JUNE

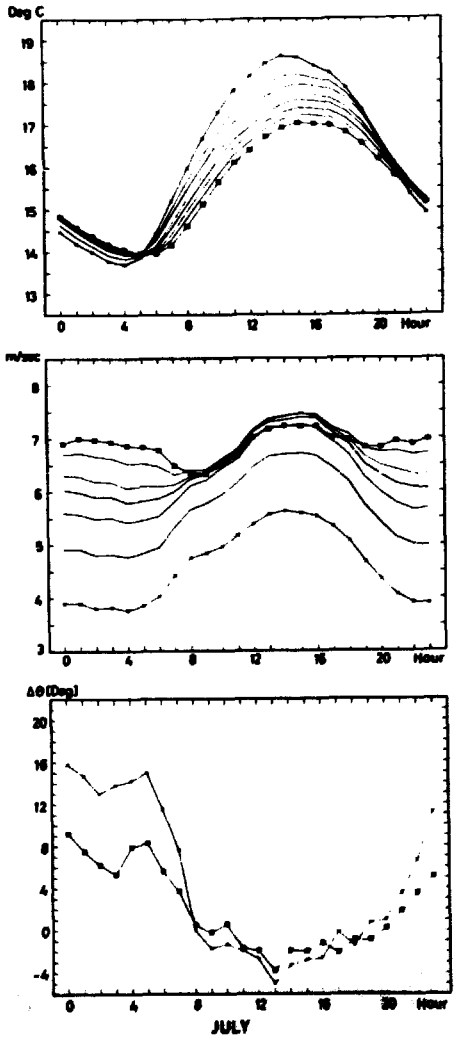
Deg C
m/sec
Δθ (Deg)
Hour
JULY

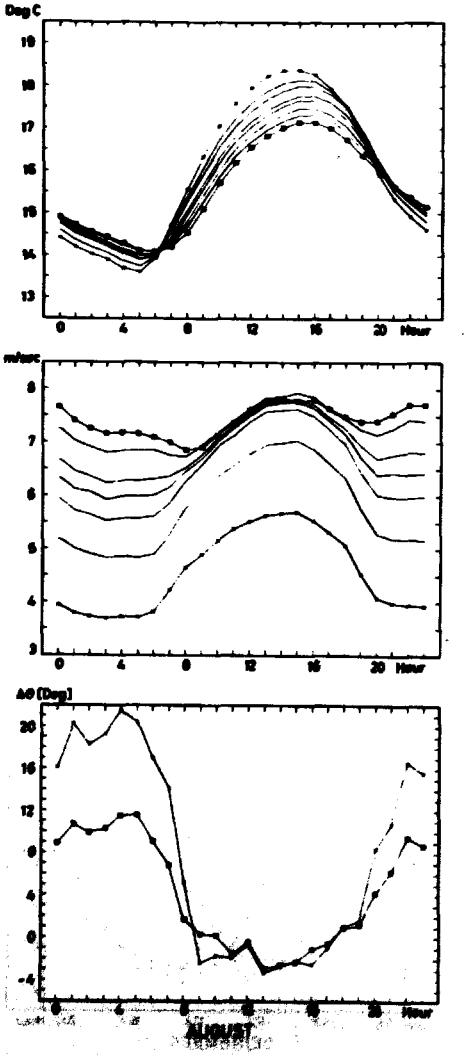
Deg C
m/sec
Δθ (Deg)
Hour
AUGUST

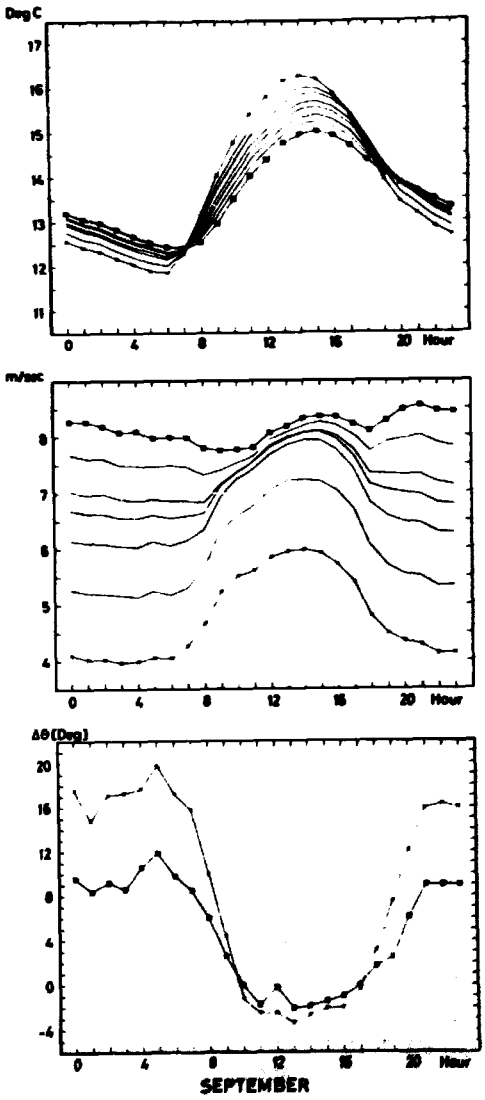
Deg C
17
16
15
14
13
12
11
0
4
8
12
16
20
Hour
m/sec
9
8
7
6
5
4
0
4
8
12
16
20
Hour
Δθ (Deg)
20
16
12
8
4
0
-4
0
4
8
12
16
20
Hour
SEPTEMBER

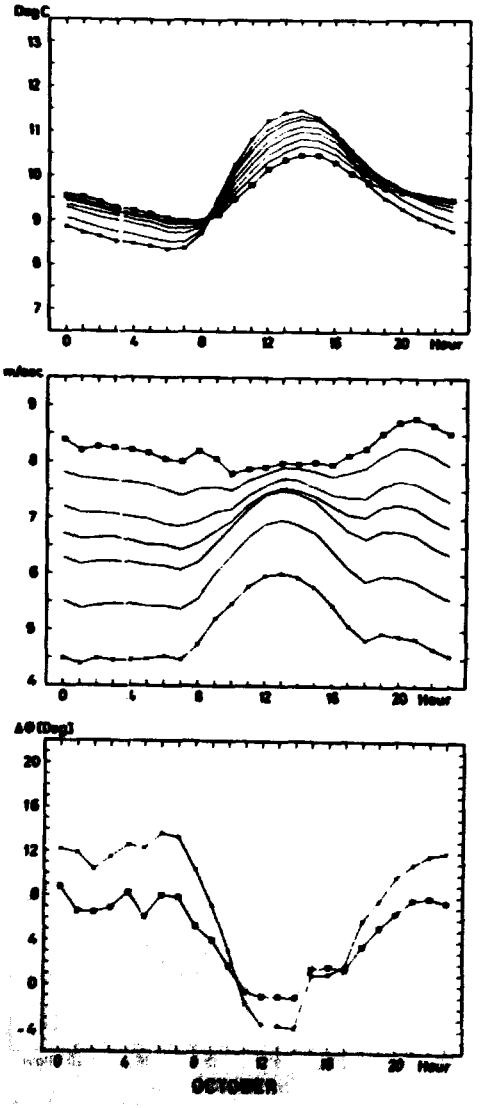
Deg C
13
12
11
10
9
8
7
0
4
8
12
16
20
Hour
m/sec
9
8
7
6
5
4
0
4
8
12
16
20
Hour
Δθ (Deg)
20
16
12
8
4
0
-4
0
4
8
12
16
20
Hour
OCTOBER

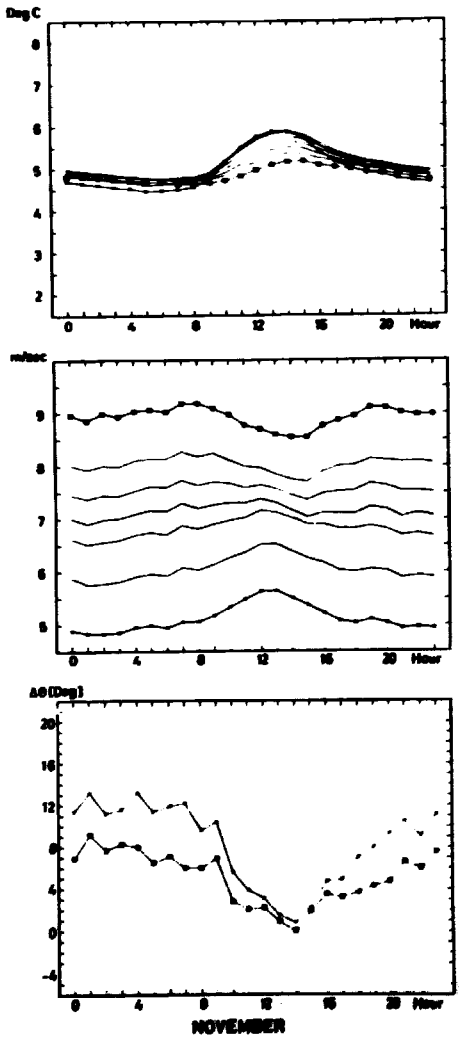
Deg C
m/sec
Δθ(Deg)
Hour
NOVEMBER

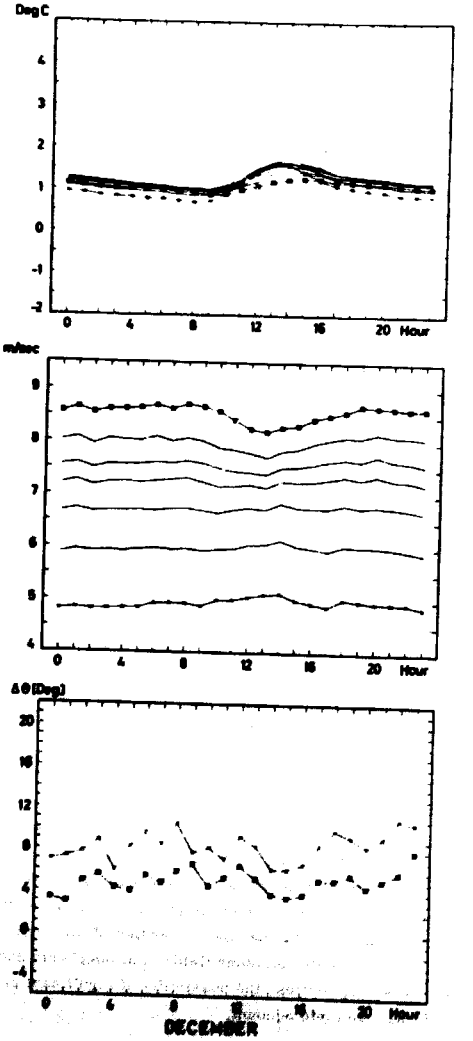
Deg C
m/sec
Δθ(Deg)
Hour
DECEMBER

SUMMARY AND CONCLUSIONS

Time series of wind speeds and wind directions measured along the Risø 123 m meteorological tower throughout ten years were analysed by spectral techniques. It was shown that the speed spectra are in good agreement with those obtained by others. However, it was further shown that an analysis of speed data alone does not realistically represent the division of the total energy into eddy energy and energy of the mean flow, and neither does such an analysis give any realistic distribution of the eddy energy over the appropriate range of frequencies. It is recommended that when kinetic energy spectra covering a huge range of periods are to be calculated, the component spectra, rather than the speed spectra should be calculated whenever possible.

Evidence and explanations were given of an almost general existence of a spectral gap between large-scale and small-scale atmospheric motions.

The diurnal and the semidiurnal peaks in the spectra were considered and it was argued that whereas the diurnal peak can easily be given a physical explanation, the semidiurnal peak may be the effect of physical processes and/or the methods of analysis.

The coordinate system was rotated in order to find the variations thus induced in the component spectra. A simple method was worked out and the results showed, in explainable contrast to other works, that the rotating of the coordinate system did not yield a totally lopsided division of energy on components.

Spectral equations in the frequency domain were derived, showing that the average spectral density of kinetic energy multiplied by frequency is given by a sum of quadrature spectra. It was shown how one of the terms in the equations could be used to determine the explicit effect of the rotating of the earth on the kinetic energy spectrum. A preliminary investigation using data from Risø and Station Nord indicated that such a type of analysis may be advantageous.

Finally, using the Risø Tower data an analysis was performed of the response of the lowest hundreds of metres of the planetary boundary layer to the diurnal variations of insolation. It was argued that several of the features observed in the measured wind profiles could be explained by horizontal inhomogeneities in the thermal properties of the surface. Thus, in order to model wind fields and other fields of atmospheric parameters over mesoscale areas, e.g. cities, the possibility of significant pressure variations should be taken into account.

ACKNOWLEDGEMENTS

The work presented in this report is selected from the research carried out by the author at the Meteorology Section of the Danish AEC Physics Department during the period from September 1970 to April 1973.

The report was completed in April 1973 in partial fulfilment of the requirements for obtaining the lic. techn. (Ph. D.) degree. However, for various reasons publication was delayed until 1975.

During my work I much benefitted from the advice and wisdom of Niels E. Busch, as well as of other colleagues at Risø, Leif Kristensen, Søren E. Larsen and Niels O. Jensen. Further, I gained much experience through collaboration with Professor Hans A. Panofsky, and Professor John A. Dutton, both of Pennsylvania State University, Professor Peter A. Taylor of the University of Southampton, and Professor Werner Klug of the Technical University of Darmstadt.

The hospitality and never failing interest of all the staff of the Meteorology Section, including Gunnar Jensen, Jørgen Christensen, Morten Frederiksen, Knud Sørensen, and Gunner Dalsgård are gratefully acknowledged.

The work was supported by the Danish Atomic Energy Commission.

I am much indebted to Professor Frank A. Engelund, The Technical University of Denmark, for his help and support.

REFERENCES

Batchelor, G.K., The Theory of Homogeneous Turbulence (Cambridge University Press, London, 1956) 197 pp.

Bendat, J.S. and A.G. Piersol, Measurement and Analysis of Random Data (John Wiley and Sons, New York, 1966) 390 pp.

Bingham, C. et al., Modern Techniques of Power Spectrum Estimation. IEEE Trans. Audio Electroacoustics, AU-15, No. 2 (1967) 56-66.

Blackadar, A.K., Periodic Wind Variations. Mineral Industries 28, No. 4, The Pennsylvania State University (1959) 1-5.

Blackadar, A.K., A single Layer Theory of the Vertical Distribution of Wind in a Baroclinic Neutral Atmospheric Boundary Layer. Final Report, Contract No. AF (604)-6641, Dept. of Meteorol. Penn. State Univ. (1965) 1-22.

Bretherton, F.P. et al., The Spectral Gap. Radio Science 4, No. 12 (1969) 1361-1363.

Busch, N.E. and H.A. Panofsky, Recent Spectra of Atmospheric Turbulence. Quart. J. Roy. Meteorol. Soc. 94 (1968) 132-148.

Busch, N.E. and E.L. Petersen, Analysis of Nonstationary Ensembles. In: Statistical Methods and Instrumentation in Geophysics. Proceedings of the NATO Advanced Study Institute in Norway April 1971. Edited by A.G. Kjelaas (Teknologisk Forlag, Oslo, 1971) 71-92.

Busch, N.E. and S.E. Larsen, Spectra of Turbulence in the atmospheric surface layer. Risø Rept. No. 256 (1972) 187-207.

Busch, N.E., On the Mechanics of Atmospheric Turbulence. Ed. D.A. Haugen. (The American Meteorological Society, 1973).

Byzova, N.L. et al., Characteristics of the Wind Velocity and Temperature Fluctuations in the Atmospheric Boundary Layer. In: Proceedings of the International Colloquium on Atmospheric Turbulence and Radio Wave Propagation, Moscow, June 1965 (Publishing House Nauka, Moscow, 1967) 76-92.

Chiu, W.C., On the Spectral Equations and the Statistical Energy Spectrum of Atmospheric Motions in the Frequency Domain. Tellus 22, 6 (1970) 606-619.

Cooley, J.W. and J.W. Tukey, J.W., An Algorithm for the Machine Calculation of Complex Fourier Series. Mathematics of Computation 19, No. 91 (1965) 297-301.

Cramer, H., On the Theory of Stationary Random Processes. Ann. Math. 41 (1940) 215-230.

Cramer, H. and M.R. Leadbetter, Stationary and Related Stochastic Processes (J. Wiley and Sons, New York, 1967) 348 pp.

Dutton, J.A., The Rate of Change of the Kinetic Energy Spectrum of Flow in Compressible Fluid. J. Atmos. Sci. 20 (1963) 107-114.

Dutton, J.A. and H.A. Panofsky, Clear Air Turbulence: A Mystery May be Unfolding. Science 167 (1970) 937-944.

Dutton, J.A., Recent Perspectives on Turbulence in the Free Atmosphere (to appear as an introduction to Turbulence in the Free Atmosphere by N.K. Vinnichenko et al. English transl. ed. by J.A. Dutton, in press, Plenum Press).

Fiedler, F. and H.A. Panofsky, Atmospheric Scales and Spectral Gaps. Bull. Amer. Meteorol. Soc., 51, No. 12 (1970) 1114-1119.

Fiedler, F., The variance Spectrum of the Horizontal Wind Velocity at 50 m above the Ground. Beiträge zur Physik der Atmosphäre 44 (1971) 187-200.

Hannan, E.J., Multiple Time Series (J. Wiley and Sons, New York, 1970) 536 pp.

Hess, S.L., Introduction to Theoretical Meteorology (Holt, Rinehart and Winston, New York, 1959) 362 pp.

Johnsen, S.J., et al., Oxygen Isotope Profiles through the Antarctic and Greenland Ice Sheets. Nature 235, No. 5339 (1972) 429-434.

Kao, S.K., Governing Equations and Spectra for Atmospheric Motion and Transports in Frequency, Wave Number Space. J. Atmos. Sci. 25 (1968) 32-38.

Kolesnikova, V.N., and A.S. Monin, Spectra of Meteorological Field Fluctuations. Izv. Acc. Sci. USSR, Atmospheric and Oceanic Physics Ser. (English translation) 1 (1965) 377-385.

Kristensen, L. and C.A. Paulson, Digital Spectrum Analysis by Use of the Fast Fourier Transform. Risø-M-1267 (1970) 51 pp.

Kristensen, L., The Effect of Aliasing, Averaging and Smoothing in Digital Spectrum Analysis. In: Statistical Methods and Instrumentation in Geophysics. Proceedings of the NATO Advanced Study Institute in Norway April 1971. Edited by A.G. Kjelaas (Teknologisk Forlag, Oslo, 1971) 1-24.

Kristensen, L. and J. Taagholt, Unmanned Geophysical Observatory at Nord in North Greenland (Danish Meteorological Institute, Copenhagen, 1973) 80 pp.

Laikhtman, D.L., Physics of the Boundary Layer of the Atmosphere (Israel Program for Sci. Transl., Jerusalem, 1964) 200 pp.

Lettau, H.H. and W.F. Dabberdt, Variangular Wind Spirals. Boundary-Layer Meteor. 1 (1970) 64-79.

Loeve, M., Probability Theory (Van Nostrand, New York, 1955) 515 pp.

Lumley, J.L. and H.A. Panofsky, The Structure of Atmospheric Turbulence (J. Wiley and Sons, New York, 1964) 239 pp.

Lumley, J.L., Stochastic Tools in Turbulence (Academic Press, New York, 1970) 194 pp.

Millard, R.C., Wind Measurements from Buoys: A Sampling Scheme. Geophys. Res. 76, No. 24 (1971) 5819-5828.

Monin, A.S. and A.M. Yaglom, Statistical Fluid Mechanics. Vol. 1 (The MIT Press, Cambridge, Massachusetts, 1971) 769 pp.

Oort, A.H. and A. Taylor, On the Kinetic Energy Spectrum near the Ground. Mon. Weather Rev. 97 (1969) 623-636.

Panofsky, H.A. and I. Van der Hoven, Spectra and Cross-Spectra of Velocity Components in the Mesometeorological Range. Quart. J. Roy. Meteorol. Soc., 81 (1955) 603-606.

Panofsky, H.A. and E.L. Petersen, Wind Profiles and Change of Terrain Roughness at Risø. Quart J. Roy. Meteorol. Soc., 98 (1972) 845-854.

Petersen, E.L. and P.A. Taylor, Some Comparisons Between Observed Wind Profiles at Risø and Theoretical Predictions for Flow over Inhomogeneous Terrain. Quart. J. Roy. Meteorol. Soc., 99 (1973) 329-338.

Peterson, E.W., Modification of Mean Flow and Turbulent Energy by a Change in Surface Roughness under Conditions of Neutral Stability. Quart. J. Roy. Meteorol. Soc. 95 (1969) 561-575.

Pettersen, S., Weather Analysis and Forecasting. (Mc Graw - Hill Book Company, Inc., New York, 1940) 503 pp.

Plate, E.J., Aerodynamic Characteristics of Atmospheric Boundary Layers. AEC Critical Review Series. TID-25465. (1971) 190 pp.

Saltzman, B., Equations Governing the Energetics of the Larger Scales of Atmospheric Turbulence in the Domain of Wave Number. J. Meteorol. 14 (1957) 513-523.

Sheih, C.M., A Theoretical Study of the Diurnal Wind Variations in the Planetary Boundary Layer. J. Atmos Sci. 29, No. 5 (1972) 995-998.

Taylor, P.A., On Wind and Shear Stress Profiles above a Change in Surface Roughness. Quart. J. Roy. Meteorol. Soc. 95 (1969) 77-91.

Thompson, R., Spectral Estimation from Irregularly Spaced Data. IEEE Transactions on Geoscience Electronics GE-9, No. 2 (1971) 107-110.

Townsend, A.A., The Structure of Turbulent Shear Flow (Cambridge Univ. Press, London, 1956) 315 pp.

Townsend, A.A., Wind and the Formation of Inversions. Atmospheric Environment 1 (1967) 173-175.

Van der Hoven, I., Power Spectrum of Horizontal Wind Speed in the Frequency Range from 0.0007 to 900 cycles per hour. J. Meteorol. 14 (1957) 160-164.

Wendell, L.W., Some Diagnostic Applications of Wind Speed and Component Spectra for Mesoscale through Synoptic Scale Frequencies. In: Proceedings of the Symposium on Air Pollution, Turbulence and Diffusion. December 1971, Edited by H.W. Church and R.E. Luna (Sandia Laboratories, Albuquerque, New Mexico, 1972) 286-293.

Wiener, N., Extrapolation, Interpolation, and Smoothing of Stationary Time Series (The M.I.T. Press, Cambridge, Massachusetts, 1949) 160 pp.

Vinnichenko, N.K., The Kinetic Energy Spectrum in the Free Atmosphere - 1 second to 5 years. Tellus 22 (1970) 158-166.

Yaglom, A.M., An Introduction to the Theory of Stationary Random Functions (Prentice-Hall, Englewood Cliffs, New Jersey, 1962) 235.